The American Journal of Pathology, Vol. 184, No. 8, August 2014

The American Journal of
PATHOLOGY
ajp.amjpathol.org

GASTROINTESTINAL, HEPATOBILIARY, AND PANCREATIC PATHOLOGY

Commensal Bacterial Endocytosis in Epithelial Cells Is Dependent on Myosin Light Chain Kinase—Activated Brush Border Fanning by Interferon-γ

Li-Ling Wu,* Wei-Hao Peng,† Wei-Ting Kuo,* Ching-Ying Huang,* Yen-Hsuan Ni,‡ Kuo-Shyan Lu,† Jerrold R. Turner,§ and Linda C.H. Yu*

From the Graduate Institutes of Physiology and Anatomy and Cell Biology,† and the Department of Pediatrics,‡ National Taiwan University College of Medicine and Hospital, Taipei, Taiwan; and the Department of Pathology,§ University of Chicago, Chicago, Illinois*

Accepted for publication
May 5, 2014.

Address correspondence to Linda C.H. Yu, Ph.D., Graduate Institute of Physiology, National Taiwan University College of Medicine, Ste. 1020, #1 Jen-Ai Rd. Sec. I, Taipei 100, Taiwan. E-mail: lchyu@ntu.edu.tw.

Abnormal bacterial adherence and internalization in enterocytes have been documented in Crohn disease, celiac disease, surgical stress, and intestinal obstruction and are associated with low-level interferon (IFN)-γ production. How commensals gain access to epithelial soma through densely packed microvilli rooted on the terminal web (TW) remains unclear. We investigated molecular and ultrastructural mechanisms of bacterial endocytosis, focusing on regulatory roles of IFN-γ and myosin light chain kinase (MLCK) in TW myosin phosphorylation and brush border fanning. Mouse intestines were sham operated on or obstructed for 6 hours by loop ligation with intraluminally administered ML-7 (a MLCK inhibitor) or Y27632 (a Rho-associated kinase inhibitor). After intestinal obstruction, epithelial endocytosis and extraintestinal translocation of bacteria were observed in the absence of tight junctional damage. Enhanced TW myosin light chain phosphorylation, arc formation, and brush border fanning coincided with intermicrovillous bacterial penetration, which were inhibited by ML-7 and neutralizing anti—IFN-γ but not Y27632. The phenomena were not seen in mice genetically deficient for long MLCK-210 or IFN-γ. Stimulation of human Caco-2BBe cells with IFN-γ caused MLCK-dependent TW arc formation and brush border fanning, which preceded caveolin-mediated bacterial internalization through cholesterol-rich lipid rafts. In conclusion, epithelial MLCK-activated brush border fanning by IFN-γ promotes adherence and internalization of normally noninvasive enteric bacteria. Transcytotic commensal penetration may contribute to initiation or relapse of chronic inflammation. *(Am J Pathol 2014, 184: 2260—2274; http://dx.doi.org/10.1016/j.ajpath.2014.05.003)*

Commensal bacteria, estimated at 100 trillion (10^{14}), are normally confined to the gut lumen and not in direct contact with epithelial cells. However, abnormal bacterial adherence and internalization in enterocytes have been documented in patients and experimental models with Crohn disease,[1,2] celiac disease,[3,4] chronic psychological stress,[5] surgical manipulation,[6] and intestinal obstruction (IO).[7] Recent *in vitro* studies have found transcellular passage of nonpathogenic, noninvasive bacteria in epithelial monolayers after exposure to inflammatory and metabolic stress, such as interferon (IFN)-γ,[8,9] hypoxia,[10] and mitochondrial damage.[11] To date, the molecular mechanisms of bacterial endocytosis in enterocytes remain unclear.

Polarized intestinal epithelial cells are endowed with densely packed apical microvilli or brush border (BB), which act as an ultrastructural barrier that impedes physical contact between enteric microbes and cellular soma.[12] However, recent findings have revealed that commensal bacteria are internalized into epithelial cells via cholesterol-rich lipid rafts situated at invaginations of apical membrane between adjacent microvilli.[8,13,14] It is still poorly understood how microbes of 0.5 to 1 μm gain access to the base of the intermicrovillous cleft. Actin-cored microvilli are rooted in the filamentous meshwork of the terminal web

Supported by National Natural Scientific Foundation grants NSC99-2320-B-002-024-MY3, NSC102-2325-B-002-035, and NSC102-2628-B-002-009-MY3 (L.C.H.Y.) and National Taiwan University grant 10R7807 (L.C.H.Y.).

Disclosures: None declared.

http://dx.doi.org/10.1016/j.ajpath.2014.05.003

(TW), which consists of multiple proteins, including actin, myosin, fodrin, and spectrin.[15] Early reports revealed that the phosphorylation of myosin light chain (MLC) in the TW region, via unknown kinases, leads to BB fanning in enterocytes.[16,17] Other studies have found that the phosphorylation of perijunctional MLC by myosin light chain kinase (MLCK) and Rho-associated kinase (ROCK) is involved in epithelial tight junction (TJ) disruption.[18,19] We hypothesized that TW MLC contraction and BB fanning may allow bacterial penetration through an enlarged intermicrovillous cleft to initiate apical endocytosis. The roles of MLCK and ROCK in mechanisms of bacterial endocytosis and their correlation with TJ changes have yet to be determined.

Previous studies from our laboratory found increased bacterial translocation (BT) to extraintestinal organs after IO by loop ligation.[20,21] The current aim was to investigate molecular and ultrastructural mechanisms of apical bacterial endocytosis in enterocytes of IO models, focusing on the role of MLCK-dependent TW myosin phosphorylation and BB fanning. The regulatory role of IFN-γ was also examined using genetically deficient mice and epithelial cell cultures.

Materials and Methods

Animals

Specific pathogen-free BALB/c and C57BL/6 male mice (6 to 8 weeks old) were obtained from the Animal Center of National Taiwan University. *MLCK*$^{-/-}$ mice (B6 background) that lacked the long 210-kDa MLCK were obtained from Dr. J. R. Turner (University of Chicago, Chicago, IL).[22] *IFN-γ*$^{-/-}$ mice (B6 background) were obtained from the Jackson Laboratory (Chicago, IL). All experimental procedures were approved by the Animal Care and Use Committee of National Taiwan University.

Surgical Procedure of IO

In the first set of experiments, mice were randomly divided to 2 groups: sham operation (sham) and IO. Both groups were sacrificed 1, 3, 6, and 24 hours after the surgical procedure. In the next set of experiments, mice were randomized to four groups: sham, IO+vehicle (veh), IO+ML-7, and IO+Y27632 (Y27). All four groups were sacrificed 6 hours after the surgical procedure.

Mice were fasted overnight but allowed to drink water ad libitum. After i.p. anesthetization with 40 mg/kg of sodium pentobarbital, mice underwent aseptic laparotomy. In the IO group, the distal small intestine was mechanically obstructed with 4-0 nylon at both ends for a 10-cm loop ligation ending 1-cm proximal to the ileocecal junction.[21] Mice in the sham group received laparotomy and mock manipulation of the gut without ligation. In all animals, care was taken not to occlude or puncture mesenteric vessels, and no sign of cyanosis was seen during the experiment. After ligation, phosphate-buffered saline (PBS) vehicle, 10 μmol/L ML-7 (a specific MLCK inhibitor; Sigma-Aldrich, St. Louis, MO), or 50 μmol/L Y27632 (a specific ROCK inhibitor; Sigma-Aldrich) was administered intraluminally in a volume of 0.25 mL using a 26-gauge needle with polyethylene tubing 10. The hole in the gut wall was closed, and the abdominal layers were sutured after surgery. The mice were placed back into steel cages, fasted but with free access to water, and sacrificed at various time points.

Blockade Studies with anti—IFN-γ

Hamster anti-mouse IFN-γ clone H22 (BioLegend, San Diego, CA) was used to neutralize IFN-γ, and hamster IgG_1 isotype antibody was used as a control.[23] After bowel ligation, mice were i.p. injected with 0, 10, 50, or 100 μg of anti—IFN-γ or 100 μg of IgG_1 isotype in 0.1 mL of sterile PBS. All mice were sacrificed 6 hours after the surgical procedure. The neutralizing effect was verified in mucosal samples using an enzyme-linked immunosorbent assay (ELISA) kit for IFN-γ (eBioscience, San Diego, CA).

Quantification of Luminal Bacteria in Small Intestines

At the time of sacrifice, the distal small intestines of mice in the sham group were ligated to a 10-cm loop as in the IO mice. The intestinal loops of sham and IO mice were excised and luminally instilled with 0.25 mL of sterile PBS through the open end. The intestinal loop was then closed tightly and the lavage solution distributed by rocking the section back and forth 10 times before drainage. The lavage was plated onto fresh blood agars for culturing, and luminal bacteria counts were expressed as $\log_{10}$ of colony-forming units (CFUs) per centimeter of intestinal segment.[21]

Analysis of BT

The liver and spleen tissues were homogenized and sonicated in sterile PBS at a ratio of 1 mg to 10 μL. Undiluted lysate (200 μL) was inoculated onto fresh blood agar plates. After incubation at 37°C for 24 hours, bacterial counts were expressed as $\log_{10}$ of CFUs per gram of tissue.[21,24]

Quantification and Classification of Epithelial Endocytosed Bacteria

Intestinal epithelial cells were isolated using a previously described protocol.[25,26] A total of 2×10^6 isolated epithelial cells were incubated with 300 μg/mL of gentamicin (Sigma-Aldrich) for 1 hour.[26] After washing, cells were lyzed with 1% Triton X-100 in PBS for 10 minutes on ice. The cell lysate was plated onto agar plates overnight at 37°C. The numbers of bacterial colonies are presented as $\log_{10}$ CFU per 10^6 cells. The individual bacterial colonies were picked out for DNA extraction and sequencing (see below).

Bacterial Profiling by Denaturing Gradient Gel Electrophoresis and 16S Ribosomal DNA Sequencing

The DNA of luminal contents in mouse small intestine was extracted using a QIAamp DNA Stool Mini Kit (Qiagen, Hilden, Germany) and subjected to polymerase chain reaction (PCR) in a T3000 Thermocycler (Biometra, Goettingen, Germany).[27] The amplification of the V2-3 variable region of the 16S ribosomal RNA gene was performed using a forward primer (5′-CGCCCGCCGCGCGCGGCGGGCGGGGCGGGGGCACGGGGGGTCCTACGGGAGGCAGCAG-3′) and a reverse primer (5′-ATTACCGCGGCTGCTGG-3′). The forward primer contains an additional 40-nucleotide GC-rich sequence (GC clamp; underlined) at the 5′ end. The PCR mixture contained 200 ng of template DNA, 1.5 μL of forward primer, 1.0 μL of reverse primer, 0.5 μL of Taq polymerase, 0.5 μL dNTPs (25 mmol/L), and 5 μL of 10× PCR buffer in a total reaction volume of 50 μL. All PCR amplifications were initiated at 94°C for 5 minutes. The samples were then denatured at 94°C for 30 seconds, followed by annealing at 53°C for 30 seconds and elongation at 72°C for 30 seconds, repeated for 35 cycles. A final elongation step at 72°C for 10 minutes was included, and the PCR products were separated on a gradient gel with denaturants.[27] The 8% (w/v) polyacrylamide solution was used to cast a gel with denaturant gradients ranging from 40% to 60% [100% corresponding to 7 mol/L urea and 40% (v/v) formamide]. Electrophoresis was performed at a constant voltage of 50 V at 60°C for 12 hours. The dominant bands were punched from the gels for DNA extraction and reamplified using the forward primer (without the GC clamp) and the reverse primer. The PCR products were subcloned into plasmids and purified. The PCR fragments were sequenced and then classified using the naive Bayesian classifier provided by the ribosomal database project.[28] Sequences from 16S gene libraries were deposited to the DNA Databank of Japan (*http://www.ddbj.nig.ac.jp*; accession numbers AB771416 to AB771423).

Fluorescent *in Situ* Hybridization

Intestinal tissues were fixed in Carnoy's solution (Ricca Chemical Company, Arlington, TX), embedded in paraffin wax, and processed according to a standard protocol.[25] Briefly, 5-μm-thick sections were mounted onto glass slides and deparaffinized. Slides were treated with 1% Triton X-100 for 90 seconds and then incubated in PBS that contained 5 mg/mL of lysozyme for 20 minutes at 37°C. Slides were rinsed thoroughly with water and air-dried. Sections were preincubated at 46°C for 60 minutes in a hybridization buffer that contained 900 mmol/L NaCl, 20 mmol/L Tris-HCl, 15% formamide, and 0.01% SDS (pH 7.4). Prewarmed hybridization buffer that contained 0.1 μmol/L oligonucleotide probe was applied to the tissue sections. These included 5′-end fluorescein isothiocyanate–labeled universal bacterial probe (EUB338) (5′-GCTGCCTCCCGTAGGAGT-3′) and negative control probe (non-EUB338) (5′-ACATCCTACGGGAGGC-3′), as well as 5′-end Cy3-labeled probes for *Lactobacillus/Enterococcus* (Lab158) (5′-GGTATTAGCACCTGTTTCCA-3′), *Escherichia coli* (Ecol1513) (5′-CACCGTAGTGCCTCGTCATCA-3′), *Staphylococcus* (STA) (5′-TCCTCCATATCTCTGCGC-3′), and *Bacteroides* (Bac 303) (5′-CCAATGTGGGGGACCTT-3′) (Genomics BioSci and Tech, Taipei, Taiwan).[29] After incubation overnight in a dark humid chamber at 46°C, slides were rinsed thoroughly with sterile double-distilled water and then stained with Hoechst dye to visualize cell nuclei. Images were captured under a fluorescence microscope.

Preparation of Fluorescent *E. coli*

The expression plasmid pRSET that contains a green fluorescent protein (GFP) was transformed into nonpathogenic competent *E. coli* BL21 (Novagen, Madison, WI) and grown on Luria-Bertani plates supplemented with 100 mg/mL of ampicillin (Sigma-Aldrich) at 37°C overnight. Single colonies were seeded into 5 mL of Luria-Bertani broth with 100 mg/mL of ampicillin and placed on an incubated shaker (200 rpm) at 37°C till the OD_{600} reached 0.6. The GFP expression in *E. coli* was induced by adding 0.1 mmol/L isopropyl β-D-1-thiogalactopyranoside for incubation of 1.5 hours. After centrifugation, the pellet was mixed with 0.5 mL glycerol and stored at −80°C until use.

Administration of Live Fluorescent Bacteria into Intestinal Loops

We resuspended 5×10^8 GFP-expressing *E. coli* (*E. coli*–GFP) in 0.25 mL of PBS and inoculated into the obstructed loop. After 1, 3, 6, and 24 hours, the intestinal segments were excised and fixed in 2% paraformaldehyde (PFA) for 30 minutes at 4°C. Tissues were snap frozen in OCT solution (Thermo, West Palm Beach, FL) and cut into 8-μm sections with a cryostat and mounted on glass slides.[21] Tissues were blocked with fetal bovine serum for 1.5 hours and incubated with 5 U/mL of phalloidin conjugated to Alexa-633 (Invitrogen, Carlsbad, CA) for 30 minutes. The slides were stained with a Hoechst dye, and images were captured under a fluorescence microscope.

Transmission Electron Microscopy and Immunoelectron Microscopy

Intestinal tissues were fixed in 2.5% glutaraldehyde in 0.1 mol/L sodium cacodylate buffer (pH 7.4) for 2 hours at 22°C and rinsed with 0.05 mol/L Tris buffer (pH 7.4) for 4 hours at 4°C. Tissues were osmicated, dehydrated in a graded ethanol series, and embedded in epoxy resin. Vibratome sections (100 μm thick) were cut and washed in Tris buffer three times. Sections (70 nm thin) were then cut and examined with a Hitachi-7100 electron microscope (Hitachi Co., Tokyo, Japan). Electron micrographs of

epithelial cells were taken at magnifications of ×6000, ×15,000, and ×30,000.[21]

For immunoelectron microscopy, 50-μm-thick vibratome sections were placed in 5% normal goat serum in 0.1 mol/L PBS for 1 hour at room temperature. Sections were incubated with a rabbit anti–caveolin-1 monoclonal antibody (1:500; Cell Signaling, Danvers, MA) for 48 hours at 4°C. After rinsing, the sections were incubated with affinity-purified biotinylated goat anti-rabbit IgG (1:200; Jackson Laboratory) for 2 hours. The sections were treated with avidin-biotin complex for 1 hour. After rinsing, sections were soaked for 10 minutes in 0.05 mol/L Tris buffer (pH 7.2), 0.0125% diaminobenzidine, and 0.35% imidazole. This was followed by 2 to 4 minutes in a fresh aliquot of diaminobenzidine mixture that had been activated with 0.003% hydrogen peroxide. Sections were washed in 0.1 mol/L sodium phosphate buffer and then dehydrated in an alcohol series followed by infiltration and embedding with propylene oxide and Epon. Sections 70 to 90 nm thin were collected onto copper mesh grids and examined with a Hitachi-7100 electron microscope at 90 kV. Controls consisted of omitting the primary antiserum, secondary antibody, or biotin-avidin complex.

Scanning Electron Microscopy

Intestinal tissue were plated on 13 mm coverslips and treated as in the static adhesion assay. Tissues on the coverslip were fixed in 2.5% glutaraldehyde in PBS for 1

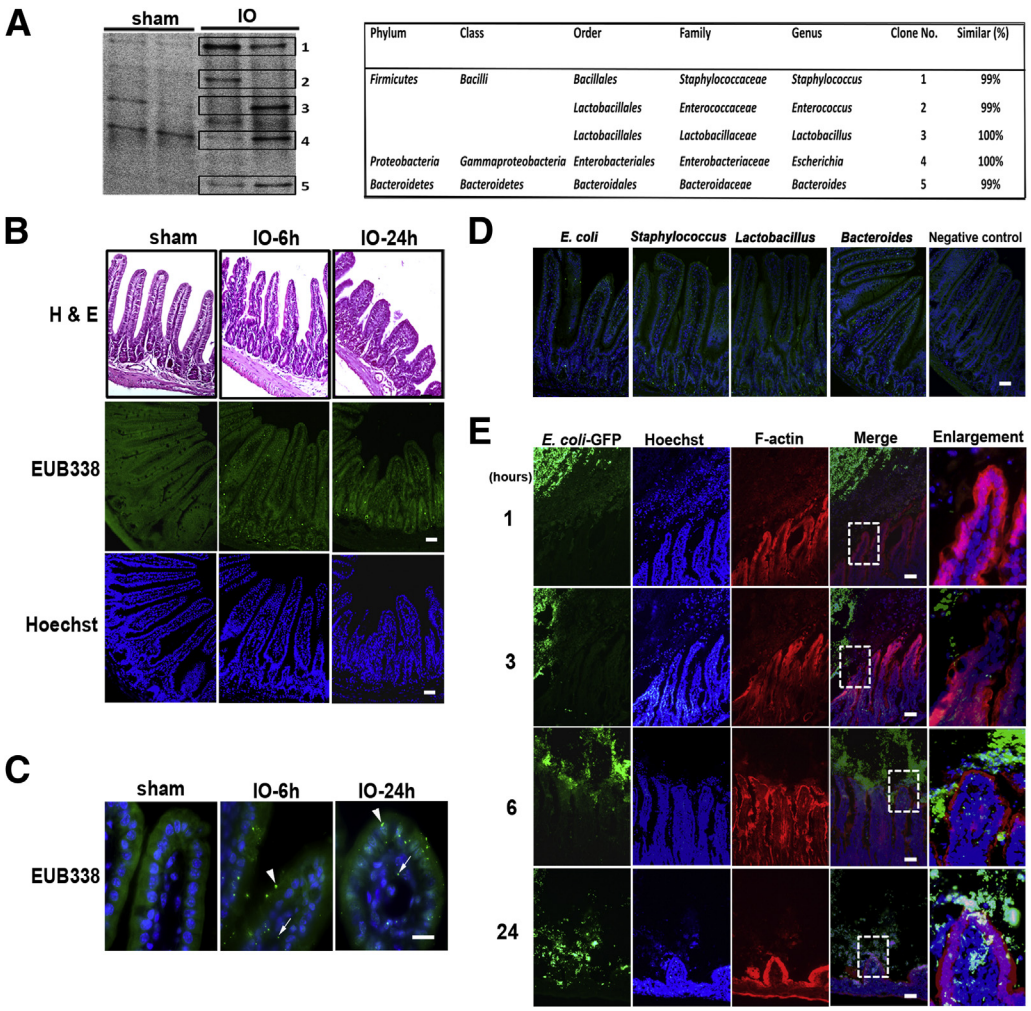

Figure 1 Mucosal adherence and penetration of enteric bacteria increases after obstruction. **A:** Analysis of bacterial strains in distal small intestines by denaturing gradient gel electrophoresis and 16S ribosomal DNA sequencing. Representative photoimage showing bands (indicated by numbers) with density change in IO mice compared with sham groups. The bacterial genus corresponding to each band number is shown. **B:** Histologic staining and bacterial hybridization in intestinal tissues of sham, IO-6h, and IO-24h mice. Intestinal sections were stained with H&E, a universal bacterial probe EUB338, or Hoechst dye. **C:** Higher magnification (×1000) showing bacteria signals in epithelial cells (**arrowheads**) and lamina propia (**arrows**) in intestinal tissues of IO-6h and IO-24h mice. **D:** The penetrated bacterial strains were characterized in IO-6h mice using specific probes targeting *Escherichia coli*, *Staphylococcus*, *Lactobacillus*, and *Bacteroides*. **E:** Temporal-spatial relationship between luminal bacteria and gut epithelium was examined by injecting 5×10^8 colony-forming units of *E. coli*–GFP into obstructed loops immediately after ligation. Superimposed images of *E. coli*–GFP (green), Hoechst (blue), and phalloidin-labeled F-actin (red) revealed bacterial attachment by 3 hours and penetration by 6 and 24 hours. Representative photomicrographs were obtained from at least four mice in each group. Scale bar = 10 μm. GFP, Green fluorescent protein; H&E, hematoxylin-eosin; IO, intestinal obstruction.

hour and then postfixed in aqueous 1% osmium tetroxide/1% tannic acid for 1 hour. After washing, samples were dehydrated in a graded ethanol series and critical point dried in a HCP-2 critical point drying device (Hitachi Co.). The specimens were mounted on metal stubs, coated with gold in a JEOL JFC-1100 Fine Coat Ion Sputter, and photographed in a scanning electron microscope (JEOL S330; JEOL Co., Tokyo, Japan).

Analysis of TW Contraction and BB Fanning

Intestinal epithelial sheets were isolated for measurement of TW contraction and BB fanning according to the methods of Keller and Mooseker.[16] Scraped mucosal samples were gently homogenized to obtain sheets of 5 to 10 epithelial cells connected by their intercellular junctions. Contraction of TW was assayed by placing the epithelial sheets in ice-cold contraction buffer with or without Ca^{2+}/ATP and immediately transferred to 37°C for 15 minutes before fixation. The epithelial sheets were photographed in a light microscope with differential interference contrast, and the width of the TW and the height of the arc were measured to determine the extent of TW contraction. For ultrastructural analysis of BB fanning, epithelial sheets were processed for transmission electron microscopy to obtain longitudinal and cross-sectional views of the BB. The extent of BB disorganization is determined according to the method of Tyska et al.[30]

Immunofluorescent Staining of p-MLC and Fodrin in Intestinal Tissues

Scraped mucosal tissues were fixed with 4% PFA for 1 hour at 4°C. The tissues were quenched with 50 mmol/L NH_4Cl (Sigma-Aldrich) in PBS for 10 minutes and blocked with fetal bovine serum for 1 hour at room temperature. After washing, tissues were incubated with rabbit anti−phosphorylated MLC2 (anti−p-MLC2) (Ser19) (1:100; Cell Signaling) and mouse anti−α-fodrin (1:100; Abcam, Cambridge, UK)

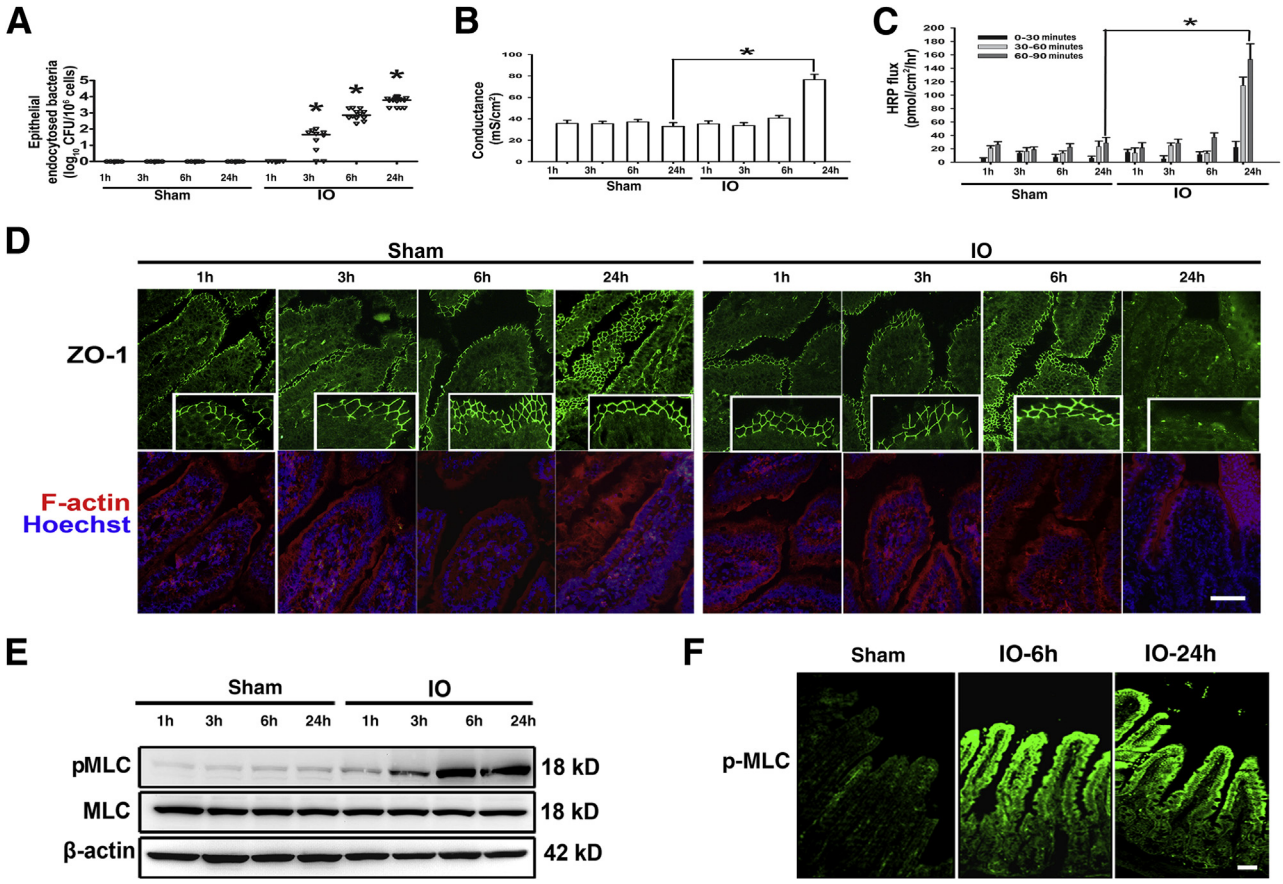

Figure 2 Bacterial endocytosis and myosin phosphorylation in epithelial cells are uncoupled with TJ damage at early time points of IO. **A:** Increased intracellular bacterial counts in enterocytes were seen as early as 3 hours and continued to increase after 6 and 24 hours of IO. The line indicates the median of each group. **B:** Intestinal tissue conductance after 3 and 6 hours of IO was comparable to those of the sham groups. The conductance value at IO-24 hours was higher than that of sham controls. **C:** Luminal-to-serosal macromolecular flux did not increase until 24 hours after IO. **D:** Photoimages showing ZO-1 staining (green) in intestinal tissues. Higher magnification (×1000) in insets revealed ZO-1 disruption at IO-24h but not early time points. Staining of F-actin (red) and cell nucleus (blue). **E:** Western blots reveal increased p-MLC in mucosal samples of IO groups after 3 to 24 hours compared with sham controls. **F:** Staining of p-MLC localizes to epithelial layers in IO mice. $n = 6$ to 8 per group. *$P < 0.05$ versus respective sham. Scale bar = 10 μm. CFU, colony-forming unit; h, hours; HRP, horseradish peroxidase; IO, intestinal obstruction; p-MLC, phosphorylated myosin light chain; TJ, tight junction; ZO-1, zonula occludens protein 1.

overnight at 4°C. The tissues were washed in PBS thrice and incubated with goat anti-rabbit IgG conjugated to Alexa-488 and anti-mouse IgG conjugated to Alexa-594 for 1 hour at room temperature. After incubating with Hoechst dye for 30 minutes, the samples were plated onto slides with an ultrathin high-performance cover glass (Zeiss, Göttingen, Germany). The slides were observed under a fluorescent microscope.

Histopathologic Examination

Intestinal tissues were fixed in 4% PFA and embedded in paraffin wax with proper orientation of the crypt to villus axis before sectioning. Sections (5 μm thick) were deparaffinized with xylene and graded ethanol, stained with hematoxylin-eosin, and observed under a light microscope.[21]

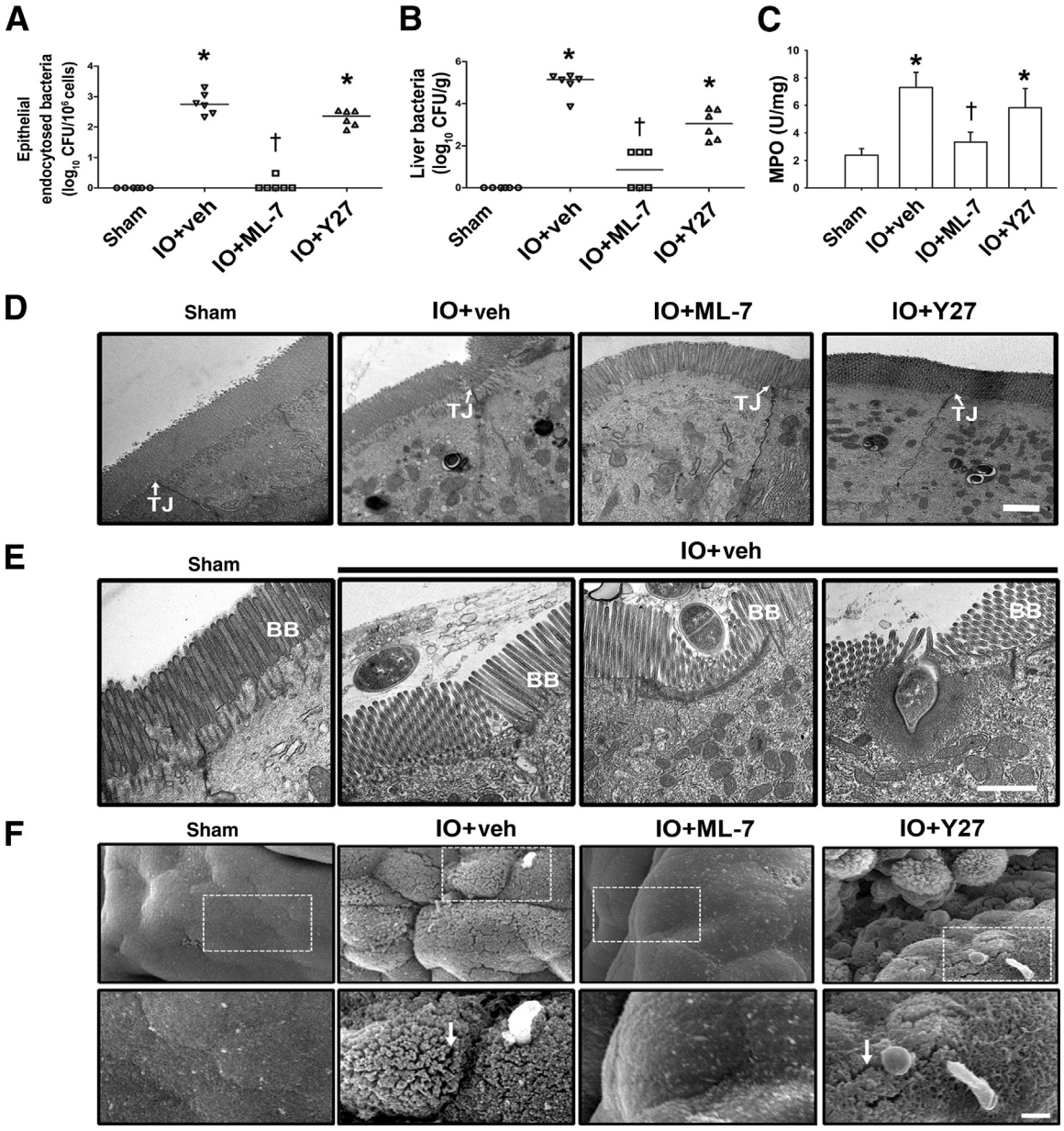

Figure 3 Epithelial endocytosis of bacteria is dependent on MLCK but not ROCK activation. Mice were intraluminally administered ML-7, Y27, or veh immediately after loop ligation, and tissues were collected 6 hours after IO. **A:** Intracellular bacterial counts decrease in enterocytes in IO mice administered ML-7 but not Y27. **B:** Liver bacterial counts reduce in IO+ML-7 but not IO+Y27 mice. **C:** Increased mucosal inflammation caused by IO is reduced by ML-7 but not Y27. **D:** Representative transmission electron micrographs showing bacterial internalization in epithelial cells of IO+veh and IO+Y27 mice but not sham and IO+ML-7 groups. Normal TJs were seen in all groups. **E:** Higher magnification (×15,000) of apical membrane and BB of enterocytes showing no sign of bacteria in sham mice, presence of bacteria in close proximity or adherent to BB, and entry into cells in IO+veh mice. **F:** Representative scanning electron micrographs showing bacterial penetration of BB of IO+veh mice but not sham controls (**upper panel**; ×3000). Higher magnification of bacteria is shown in **lower panels** (×6000). In contrast to the flat BB carpets in sham mice, multiple dome structures with enlarged crevices (**arrows**) are observed in IO+veh groups. The ultrastructural change was inhibited by ML-7 but not Y27. All representative images were obtained from at least four mice per group. $n = 6$ per group. *$P < 0.05$ versus sham; †$P < 0.05$ versus IO+veh. Scale bar = 1 μm. BB, brush border; CFU, colony-forming unit; IO, intestinal obstruction; MLCK, myosin light chain kinase; MPO, myeloperoxidase; ROCK, Rho-associated kinase; TJ, tight junction; veh, vehicle; Y27, Y27632.

Western Blotting

Intestinal mucosal proteins were extracted with complete radioimmunoprecipitation assay buffer and subjected to SDS-PAGE (4% to 13% polyacrylamide) as described.[21] The resolved proteins were then electrotransferred onto polyvinylidene difluoride or nitrocellulose membranes in a semidry blotter. Blots were blocked with 5% (w/v) nonfat dry milk in Tris-buffered saline (TBS) or 5% (w/v) bovine serum albumin in TBS with Tween 20 [0.1% (v/v) Tween 20 in TBS] for 1 hour, washed with TBS with Tween 20, and incubated with a primary antibody at 4°C overnight. The membrane was washed and incubated with a secondary antibody for 1 hour. After washing, the membranes were incubated with chemiluminescent solution and signals detected.

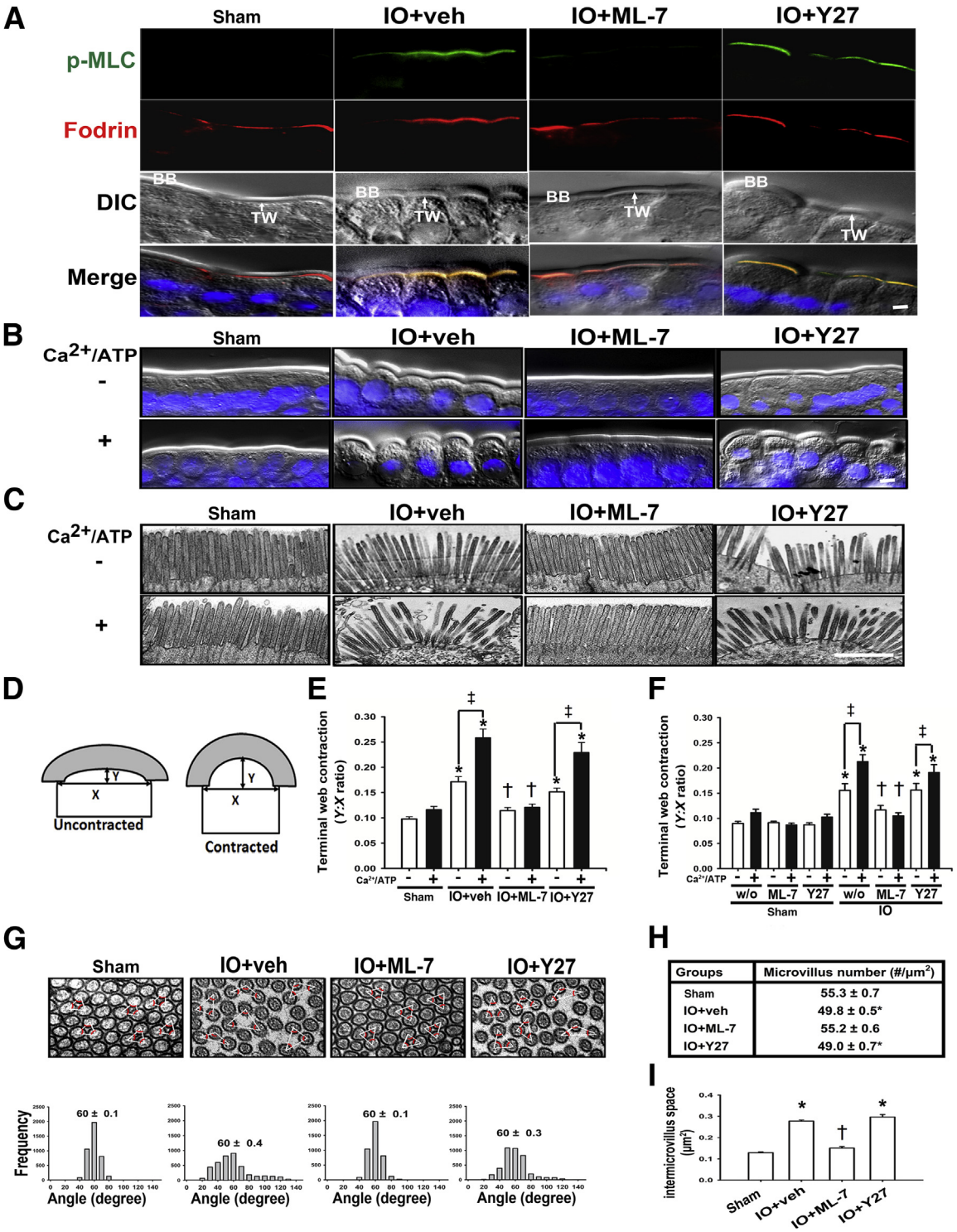

The primary antibodies used included anti-MLC (1:500; Cell Signaling), anti−p-MLC (1:500; Cell Signaling), anti−β-actin (1:10,000; Sigma-Aldrich), and anti-MLCK (1:500; Santa Cruz, Dallas, TX). The secondary antibodies used were horseradish peroxidase (HRP)−conjugated goat anti-mouse IgG (1:2000; Santa Cruz Biotechnology) and anti-rabbit IgG (1:1000; Cell Signaling).

Staining of TJs on Intestinal Tissues

A 1-cm intestinal segment was fixed with 4% PFA and then snap frozen in OCT solution. The tissues were cut into 6 μm sections with a cryostat and mounted on precoated glass slides as previously described.[21] Briefly, sections were prefixed in cold acetone, air-dried, and fixed again with 4% PFA. The tissues were permeabilized with 1% Triton X-100 for 1 minute, blocked with fetal bovine serum for 1.5 hours, and then incubated with rabbit anti−zonula occludens protein 1 (1:100; Invitrogen) at 4°C overnight. After washing, tissues were incubated with goat anti-rabbit IgG conjugated to Alexa-488 for 1 hour. The slides were washed and stained with Hoechst dye for imaging under a fluorescence microscope.

Ussing Chamber Studies and Permeability Assay

Intestinal segments (1 cm) were opened along the mesenteric border and mounted in Ussing chamber systems (World Precision Instruments, Sarasota, FL) to measure the tissue conductance as previously described.[21] The intestinal epithelial permeability was determined by the mucosal-to-serosal flux rate of HRP (mol. wt., 44 kDa; Sigma-Aldrich). Briefly, HRP was added to the luminal buffer at a final concentration of 5×10^{-5} mol/L. Then 200-μL serosal samples were collected after 0, 30, 60, and 90 minutes, and the enzymatic activity of HRP was measured. The HRP fluxes were calculated according to a standard formula and were expressed as picomoles per square centimeter per hour.[21,31]

Cell Culture Models and Bacterial Internalization Assays

Human Caco-2 epithelial cells (clone C2BBe) were seeded on 12-well transwells with filter membranes of with a pore size of 3.0 μm (2×10^5 cells/mL) and grown for 14 days until postconfluency to develop TJs and long BB.[15,32] The cells were basolaterally treated with recombinant IFN-γ (100 IU/mL) for 48 hours and processed for bacterial assays. In some experiments, 20 μmol/L ML-7 and 50 μmol/L Y27632 were added before IFN-γ treatment. In another setting, at the end of IFN-γ treatment, cell monolayers were apically administered with 2 μmol/L filipin (Sigma-Aldrich) or 50 mmol/L methyl-β-cyclodextrin (Sigma-Aldrich) 30 minutes before the bacterial assays. The amount of BT and internalization in cells was determined using the method described by Clark et al.[8] Briefly, 2×10^8 CFU/mL of fluorescent *E. coli−GFP* was inoculated into the apical chamber of transwells and incubated with cells for 1 hour, and the bacterial numbers in basolateral solution and epithelial cells were determined.[8]

Transepithelial Electrical Resistance and Paracellular Permeability

The transepithelial electrical resistance of cells was measured using an electrovoltohmeter before and after IFN-γ treatment. The paracellular permeability was determined by apical-to-basal transport of a dextran−fluorescein isothiocyanate probe (mol. wt., 3000) (Invitrogen) as previously described.[21,33]

ELISA-Based MLCK *in Vitro* Kinase Activity

MLCK activity was determined using the method described by Al-Sadi et al,[34] with slight modification. Cells were rinsed once with PBS and lyzed with radioimmunoprecipitation assay buffer. The supernatant of the cell lysates was adjusted to 5 mg/mL for the measurement of MLCK activity. Biotinylated MLC was diluted in PBS and used to coat streptavidin 96-well plates at 37°C for 1 hour. After washing with PBS, the plates were incubated with blocking solution (1 mg/mL of BSA in PBS) at 37°C for 1 hour and then washed with PBS. Kinase reaction buffer (90 μL), provided by the manufacturer (MBL International, Woburn, MA), and 10 μL of treated samples were added to the wells, and the kinase reaction was performed at 37°C for 30 to 60 minutes. The reaction was stopped by removing the reaction mixtures. The plates were rinsed three times with washing buffer and incubated with 5 ng/mL of anti− pMLC-S19 antibody at room temperature for 1 hour. After rinsing the plates, goat anti-rabbit IgG antibody (1:2000) was added to the wells for incubation at 37°C for 1 hour. After

Figure 4 MLCK-dependent TW myosin phosphorylation and arc formation correlate with BB disarray and fanning. **A:** p-MLC colocalizes with fodrin in TW of epithelial cells in IO+veh mice, which is inhibited by ML-7 but not Y27. **B:** Staining of p-MLC (green), fodrin (red), and cell nucleus (blue) is merged with DIC images to show orientation. The ultrastructures of BB, TW, and Nu are labeled. DIC images show TW arc formation on BB of IO+veh mice but not sham controls, in which the phenomenon is inhibited by ML-7 but not Y27. **C:** The arc formation in epithelial sheets was potentiated by addition of Ca^{2+}/ATP in the contraction buffer. Electron micrographs showing BB fanning in IO+veh mice, which was potentiated by addition of Ca^{2+}/ATP. **D:** The fanning is reduced in IO+ML-7 but not IO+Y27 mice. Scheme of the width (*X*) and the height (*Y*) of the TW arc in uncontracted and contracted conditions. **E:** The *Y:X* ratio was quantified to determine TW contraction. The extent of TW contraction was augmented in IO+veh mice compared with sham controls, in which the addition of Ca^{2+}/ATP caused a further increase. **F:** The contraction level is decreased in IO+ML-7 but not IO+Y27 mice. Quantification of TW contraction in epithelial sheets obtained from sham and IO+veh mice with *ex vivo* treatment with inhibitors. **G:** Representative electron micrographs showing cross-sectional view of microvilli, in which the packing angles were quantified. **H:** Disarray of BB was seen in IO+veh and IO+Y27 mice but not sham and IO+ML-7 mice. The microvillus number per area of intestinal tissues is given. **I:** The intermicrovillous space in windows of electron micrographs. $n = 5$ per group. $^*P < 0.05$ verus sham; $^\dagger P < 0.05$ versus IO+veh; $^\ddagger P < 0.05$ after addition of Ca^{2+}/ATP. Scale bar = 1 μm. BB, brush border; DIC, differential interference contrast; IO, intestinal obstruction; MLCK, myosin light chain kinase; Nu, nucleus; p-MLC, phosphorylated myosin light chain; TW terminal web; veh, vehicle; w/o, without; Y27, Y27632.

rinsing, the plates were incubated with substrate solution (tetramethylbenzidine) at 37°C for 5 to 15 minutes. A stop solution that contained 0.5 N H_2SO_4 was added, and the absorbance was determined at 450 nm using a spectrometer.

RNA Interference—Mediated Knockdown of MLCK or Caveolin-1

Cells were seeded at 2×10^5 cell/mL and transfected at 60% to 80% confluency the next day. Fifty-nanomolar siRNA in Opti-MEM RNAiMAx reagent (Santa Cruz Biotechnology) was added to cells in serum-free medium for overnight incubation. Cells were trypsinized and reseeded at 1×10^6 cells/mL on inserts of 12-well transwells. After 2 days, IFN-γ was added basolaterally for 48 hours of incubation followed by bacterial internalization assays.

Immunofluorescent Staining and Confocal Microscopy

The cell monolayer after exposure to *E. coli*—GFP was processed for immunofluorescent staining. The cells on filter supports were fixed with 4% PFA, permeabilized with 0.5%

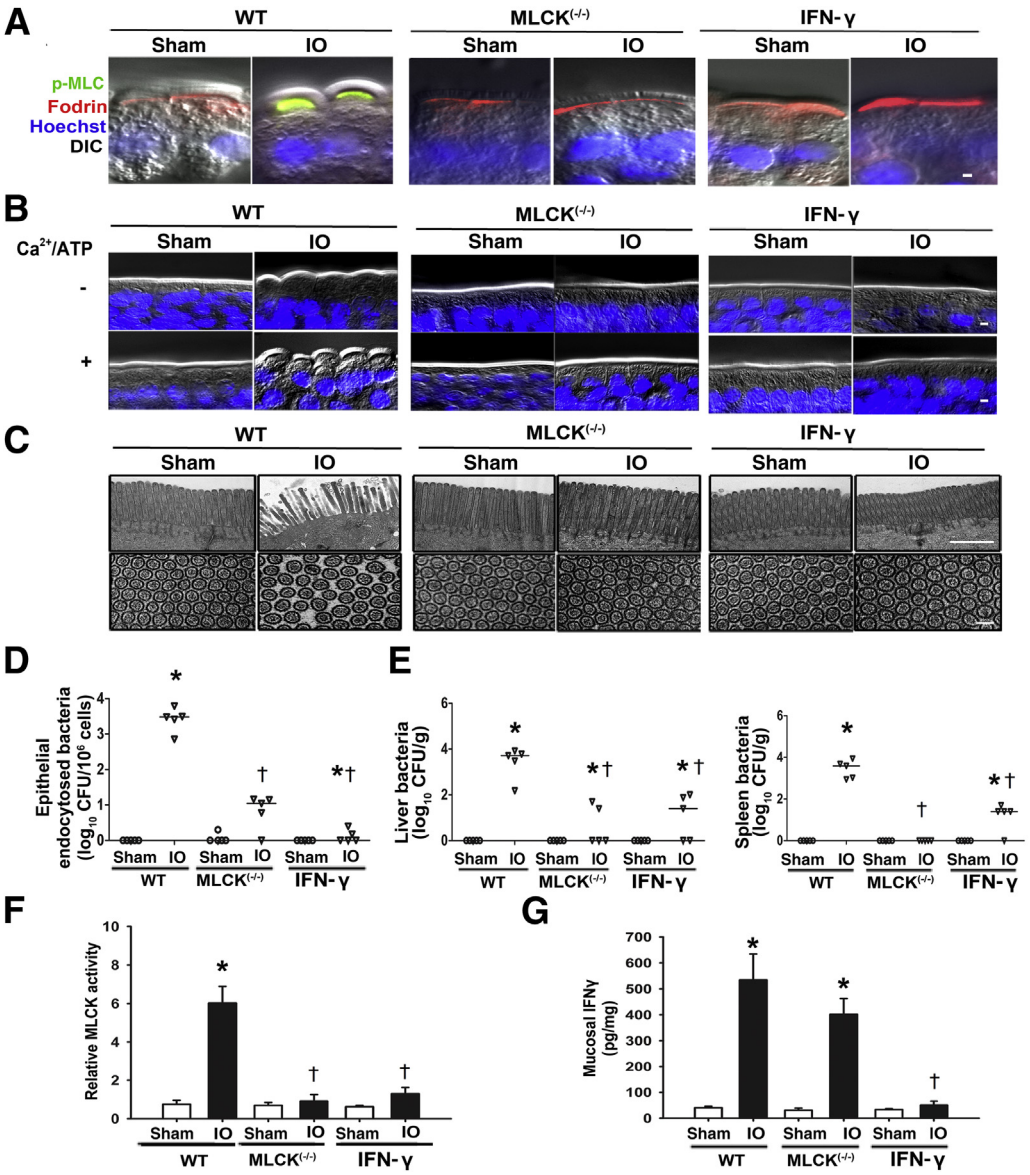

Figure 5 TW-associated BB fanning and bacterial endocytosis are absent in enterocytes of MLCK$^{-/-}$ and IFN-γ$^{-/-}$ mice. **A:** p-MLC in TW of epithelial cells is seen after IO in WT but not mutant mice. **B:** Staining of p-MLC (green), fodrin (red), and cell nucleus (blue) is merged with DIC images to show orientation. TW arc formation caused by IO is seen in WT but not mutant mice and is potentiated by addition of Ca^{2+}/ATP. **C:** Electron micrographs of longitudinal and cross-sectional views of BB show IO-induced BB fanning in WT mice and attenuation of fanning in mutant mice. Bacterial counts decrease in intestinal epithelial cells of MLCK$^{-/-}$ and IFN-γ$^{-/-}$ mice (**D**) and in liver and spleen tissues of MLCK$^{-/-}$ and IFN-γ$^{-/-}$ mice (**E**). **F:** MLCK activity increases after IO in WT mice but not mutant mice. **G:** Mucosal IFN-γ levels increase after IO in WT and MLCK$^{-/-}$ mice but not IFN-γ$^{-/-}$ mice. $n = 6$ per group. $^*P < 0.05$ versus respective sham; $^\dagger P < 0.05$ versus IO in WT mice. Scale bar = 1 μm. BB, brush border; CFU, colony-forming unit; DIC, differential interference contrast; IFN-γ, interferon-γ; IO, intestinal obstruction; MLCK, myosin light chain kinase; p-MLC, phosphorylated myosin light chain; TW terminal web; WT, wild type.

Triton X-100, and quenched with 50 mmol/L NH_4Cl. After blocking with 1% BSA, cells were stained with mouse monoclonal anti− zonula occludens protein 1 conjugated with Alexa-594 (1:100; Invitrogen) or with phalloidin conjugated to Alexa-594 (5 U/mL; Invitrogen) to visualize F-actin. The cell nuclei were stained with Hoechst dye. The filter support was cut off and mounted on slides, and images were captured using a laser scanning confocal microscope (Zeiss LSM780).

Statistical Analysis

All data are expressed as means ± SEM, except that bacterial CFU values were presented as medians. When normality assumption was appropriate, data were analyzed by one-way analysis of variance, followed by the Student-Newman-Keuls method for multiple comparisons. When comparing the difference between two groups of bacterial CFU values that failed to satisfy the normality assumption, the nonparametric *U*-test

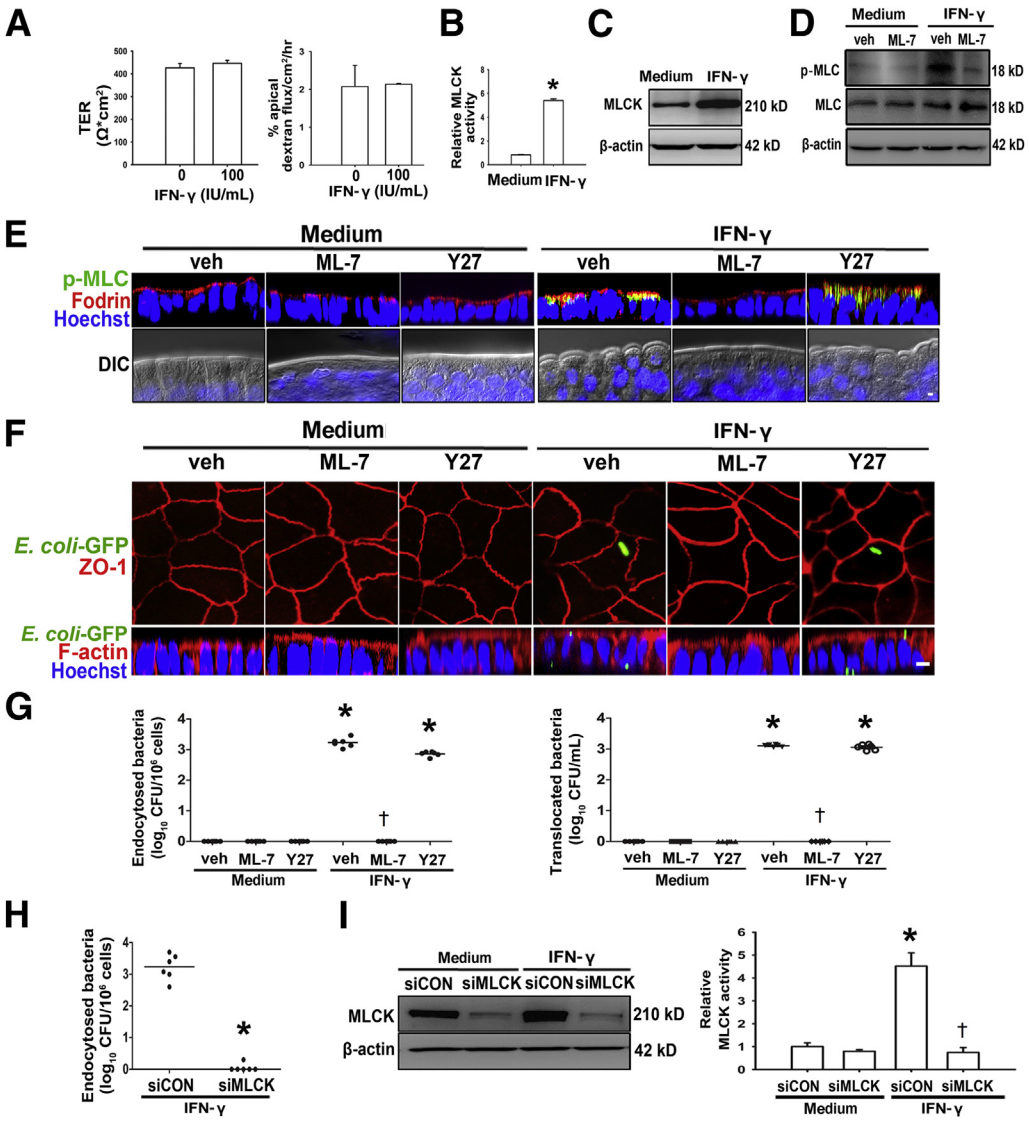

Figure 6 IFN-γ triggers MLCK-dependent ROCK-independent TW myosin phosphorylation and bacterial endocytosis in human epithelial Caco-2 cells. **A:** Caco-2 cells serosally treated with IFN-γ for 48 hours do not show changes in TER and dextran flux. **B:** Treatment with IFN-γ increases MLCK activity. **C:** IFN-γ increases the expression levels of MLCK in cells. **D:** IFN-γ enhances MLCK-dependent MLC phosphorylation. **E:** TW myosin phosphorylation parallels arc formation after IFN-γ treatment, which is inhibited by ML-7 but not Y27. Superimposed images of p-MLC (green) and fodrin (red) staining and DIC images of epithelial monolayer with cell nuclei (blue). **F:** Confocal images show adherence and internalization of *E. coli*—GFP (green) in IFN-γ—treated cells with intact tight junctions, ZO-1 (red). **G:** The phenomenon is inhibited by ML-7 but not Y27. Bacterial endocytosis and transcytosis increases after exposure to IFN-γ compared with medium, which is inhibited by ML-7 but not Y27. **H:** Transfection with siMLCK decreases IFN-γ—induced bacterial endocytosis compared with siCON. **I:** Reduction of protein expression and activity level of MLCK confirms the efficiency of gene silencing. $n = 6$ per group. $^*P < 0.05$ versus medium; $^\dagger P < 0.05$ versus veh (**G**) or siCON (**H**). Scale bar = 1 μm. CFU, colony-forming unit; DIC, differential interference contrast; IFN-γ, interferon-γ; MLCK, myosin light chain kinase; ROCK, Rho-associated kinase; siCON, siRNA to control; siMLCK, siRNA to MLCK; TER, transepithelial electrical resistance; TW, terminal web; veh, vehicle; Y27, Y27632; ZO-1, zonula occludens protein 1.

was used (Sigma Plot version 10.0; Systat Software Inc., San Jose, CA). $P < 0.05$ was considered statistically significant.

Results

Enteric Bacterial Overgrowth Coincides with Extraintestinal Translocation After Obstruction

A mouse model of IO was used to investigate the mechanisms of transepithelial bacterial penetration by loop ligation in the distal small intestine for 1, 3, 6, and 24 hours. The bacterial counts in the gut lumen, and liver and spleen tissues increased with time in IO mice compared with sham controls (Supplemental Figures S1 and S2). Bacterial DNA was extracted from luminal aspirate of the obstructed loops after 6 hours and processed for 16S ribosomal DNA sequencing, where the strains included *Staphylococcus, Enterococcus, Lactobacillus, Escherichia,* and *Bacteroides* (Figure 1A). Mucosal penetration of microbes was evident after 6 and 24 hours of IO by hybridization using primers that targeted specific bacterial strains (Figure 1, B–D). Although mucosal morphologic findings were histologically normal 6 hours after IO, villous blunting was found after 24 hours (Figure 1B).

Additional experiments by inoculating live fluorescent bacteria into ligated loops allowed us to visualize the temporal-spatial association of enteric bacteria and gut mucosa after obstruction. The *E. coli*-GFP remained in the lumen separated from epithelial layers after 1 hour, formed a close contact with epithelial surfaces after 3 hours, and penetrated into the lamina propria after 6 and 24 hours (Figure 1E).

Epithelial Adherence and Endocytosis of Commensal Bacteria Is Uncoupled with TJ Damage

The transepithelial routes of bacterial penetration were next investigated. The intracellular bacterial number in epithelial cells was significantly increased after 3, 6, and 24 hours of IO compared with respective sham controls (Figure 2A). Although no sign of paracellular permeability change was found at 6 hours of IO, elevated tissue conductance and macromolecular flux associated with TJ disruption were noted at 24 hours of IO (Figure 2, B–D, and Supplemental Figure S3). Furthermore, epithelial MLC phosphorylation levels were significantly augmented at both 6 hours and 24 hours of IO (Figure 2, E and F). Our results suggest that the onset of bacterial internalization and MLC phosphorylation in enterocytes were earlier than the increase in paracellular permeability. Therefore, all of the following experiments were conducted at 6 hours of IO.

To assess the strains and diversity of endocytosed microbes, bacterial colonies derived from lyzed epithelial cells of IO mice were either subjected to Gram staining or DNA extraction. On the basis of the results of Gram staining, the percentages of colonies classified as Gram-positive rods and cocci and Gram-negative rods and cocci were 19%, 12%, 35%, and 31%, respectively. In addition, 3% of the bacterial clones were unclassified and unidentified. According to the data of 16S ribosomal DNA sequencing, multiple strains of commensal bacteria (ie, *Bacillus, Enterococcus, Staphylococcus, Escherichia,* and *Acinetobacter*) were present within enterocytes.

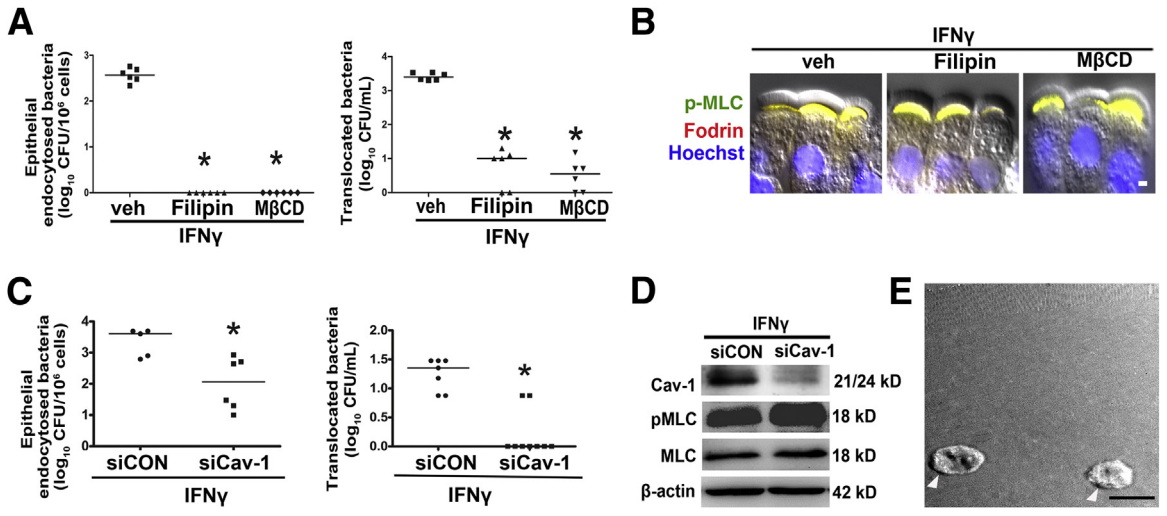

Figure 7 Myosin phosphorylation and arc formation of TW precedes Cav-1–dependent bacterial internalization through cholesterol-rich lipid rafts. **A:** Administration of cholesterol-sequestering agents (filipin and MβCD) decreases IFN-γ–induced bacterial endocytosis and translocation compared with veh controls. **B:** Filipin and MβCD have no effect on IFN-γ–induced MLC phosphorylation and arc formation of TW. **C:** Staining of p-MLC (green), fodrin (red), and cell nucleus (blue) is merged with DIC images to show orientation. Transfection with siCav-1 decreases IFN-γ–induced bacterial endocytosis and translocation compared with siCON. **D:** Western blots confirm the reduction of Cav-1 levels by gene silencing. **E:** IFN-γ–induced MLC phosphorylation does not decrease by siCav-1. Electron microscopic images show colocalization of bacteria and caveolin-1 (**arrowheads**) in intestinal epithelial cells of IO mice, by immunostaining with anti–Cav-1 monoclonal antibody. $n = 6$ per group. $^*P < 0.05$ versus veh or siCON. Scale bar = 1 μm. Cav-1, caveolin-1; CFU, colony-forming unit; DIC, differential interference contrast; IFN-γ, interferon-γ; IO, intestinal obstruction; MβCD, methyl-β-cyclodextrin; MLC, myosin light chain; p-MLC, phosphorylated myosin light chain; siCav-1, siRNA to caveolin-1; siCON, siRNA to control; TW, terminal web; veh, vehicle.

By using real-time imaging, we observed live motile bacteria in the gut lumen separated from epithelial surfaces by a thick static mucous layer in sham controls (Supplemental Video S1 and Supplemental Figure S4). In contrast, dynamic bacterial penetration through a turbulent, fluid mucous layer was seen in intestinal samples of IO mice (Supplemental Video S2 and Supplemental Figure S4). The presence of the glycoprotein-rich mucous layer covering epithelial surfaces in both groups was confirmed by Alcian blue periodic acid-Schiff staining (Supplemental Figure S4).

Bacterial Endocytosis is Dependent on MLCK Activation Associated with TW Contraction and BB Fanning

Because epithelial MLC hyperphosphorylation paralleled bacterial endocytosis in the early phases of IO, we sought to determine the roles of MLCK and ROCK in mechanisms of bacterial internalization. Intraluminal administration of ML-7 prevented the increase in intracellular bacterial counts in isolated enterocytes of IO mice, whereas treatment with Y27632 had no effect (Figure 3A). The extraintestinal bacterial counts and mucosal MPO activity were also decreased in mice treated with ML-7 but not Y27632 (Figure 3, B and C). Comparable levels of gut luminal bacterial counts were seen in IO mice given vehicle, ML-7, or Y27632, ruling out bactericidal effects of pharmacologic inhibitors (Supplemental Figure S5A).

Electromicrographic images revealed that enteric bacteria were not in close contact with BB of epithelial cells in sham controls (Figure 3, D and E). By contrast, the presence of adherent and internalized bacteria within enterocytes was observed in IO mice (Figure 3, D and E). Using scanning electron microscopy, we noted bacterial attachment on multiple bouquet-like dome structures on villous surface of IO mice compared with the smooth villous exterior without bacteria in sham controls (Figure 3F). In addition, enlarged crevices were seen on the BB carpet in IO groups (Figure 3F). These morphologic changes were inhibited by ML-7 but not Y27632 (Figure 3F), suggesting an MLCK-dependent mechanism.

We next examined whether MLCK-dependent phosphorylation is involved in TW arc formation and BB fanning in IO enterocytes. Compared with sham controls, heightened amounts of p-MLC colocalized with fodrin staining (an indicator of the TW region) in isolated epithelial sheets in IO mice (Figure 4A). The increase in the TW p-MLC level was inhibited in mice administered ML-7 but not Y27632 (Figure 4A). By high-resolution imaging and electron microscopy, a smooth lining of BB formed by highly organized microvilli was seen in epithelial sheets of sham controls, whereas TW arc formation and BB disarray were observed in those of IO mice (Figure 4, B and C). *Ex vivo* addition of calcium/ATP to epithelial sheets further potentiated the arc formation in IO groups (Figure 4, B and C). To quantify TW contraction, ratios of the height and width of the arc in each enterocyte were determined as shown in the scheme (Figure 4D). Totals of 140% and 210% were seen in IO groups compared with sham controls in calcium/ATP-free and -containing solutions, respectively (Figure 4E). *In vivo* and *ex vivo* administration with ML-7 blocked the epithelial TW contraction in IO mice (Figure 4, E and F). On the other hand, Y27632 had no effect.

The organization of BB was further examined by quantifying the packing angles of microvilli and intermicrovillous space. Densely packed microvilli were seen in the cross-sectional view of BB in sham controls, whereas a poor organization was observed in that of IO mice (Figure 4G). A wider range of packing angles of microvilli was seen in IO mice compared with sham controls (Figure 4G). A decrease in microvillus numbers and increase in intermicrovillous space per surface area were noted in IO mice compared with sham controls (Figure 4, H and I). The disorganized pattern of BB caused by IO was inhibited by ML-7 but not Y27632 (Figure 4, H and I).

IFN-γ Is Involved in Mechanisms of Epithelial MLCK-Dependent TW Phosphorylation and Bacterial Endocytosis

A 2.5-times increase in mucosal IFN-γ levels was observed in IO mice compared with sham controls (Supplemental Figure S6A). Administration of neutralizing anti−IFN-γ decreased the epithelial TW p-MLC levels (Supplemental Figure S6, B and C), and reduced BB fanning in IO mice (Supplemental Figure S6, D−G). Lower counts of endocytosed and translocated bacteria were found in mice administered anti−IFN-γ versus isotypes (Supplemental Figure S6, H and I). Anti−IFN-γ did not affect the luminal bacterial counts (Supplemental Figure S5B).

Additional experiments were conducted in mice deficient in IFN-γ and long MLCK (210 kDa) to confirm their roles in epithelial bacterial endocytosis. Significant decreases in the extent of TW p-MLC and arc formation (Figure 5, A and B) and BB fanning (Figure 5C) were seen in mutant mice compared with wild types. The IO-increased counts of endocytosed and translocated bacteria were also reduced in mutant mice (Figure 5, D and E). Comparable levels of gut luminal bacterial counts were seen between mutant mice and wild types (Supplemental Figure S5C). In contrast to the increases in mucosal MLCK activity and IFN-γ levels by IO in wild-type mice, $MLCK^{-/-}$ mice had increased IFN-γ but no sign of MLCK activation, whereas $IFN\text{-}\gamma^{-/-}$ mice had the lack of both after IO (Figure 5, F and G). Collectively, our results confirmed that IFN-γ activates MLCK-dependent myosin phosphorylation in TW and bacterial transcytosis in enterocytes.

IFN-γ Induces MLCK-Dependent TW Myosin Phosphorylation Preceding Caveolin-Mediated Bacterial Internalization through Lipid Rafts in Caco-2BBe Cells

Caco-2BBe cells were used to further investigate the molecular mechanisms of bacterial internalization. Cells treated

with 100 U/mL of IFN-γ had no change in paracellular permeability (Figure 6A) but had heightened MLCK-dependent MLC phosphorylation associated with TW arc formation (Figure 6, B–E). After apical addition of *E. coli*–GFP, bacterial adherence and internalization were observed without TJ changes in IFN-γ–treated cells (Figure 6F). Importantly, no sign of bacterial attachment was seen in medium control groups (Figure 6F). A significant increase in endocytosed and translocated bacterial counts was noted in IFN-γ–treated cells (Figure 6G). All of the aforementioned phenomena were inhibited by ML-7 but not Y27632 (Figure 6, E–G). Moreover, gene silencing of MLCK by siRNA also attenuated the IFN-γ–induced increase in bacterial endocytosis (Figure 6H). Knockdown efficiency was confirmed by decreased expression and activity of MLCK (Figure 6I).

Lastly, cholesterol-sequestering agents (eg, filipin and methyl-β-cyclodextrin) and gene silencing of caveolin-1 decreased IFN-γ–induced bacterial endocytosis and transcytosis (Figure 7, A and C) but did not affect the level of MLC phosphorylation and arc formation of TW (Figure 7, B and D). These results suggest that BB fanning precedes the lipid raft–mediated bacterial internalization. None of the inhibitors or chemical agents decreased the transepithelial electrical resistance values of cell monolayers (Supplemental Figure S7).

Discussion

Abnormal commensal penetration plays a critical role in the pathogenesis of chronic intestinal inflammation and gut-derived septic complications. Recent data indicate that epithelial cells may apically internalize and transcytose bacteria, before TJ impairment, via unknown mechanisms.[8,14] Our novel findings indicate that MLCK-activated TW myosin phosphorylation and BB fanning by IFN-γ stimulation allows bacterial penetration through intermicrovillous clefts for endocytosis. The bacterial transcytotic route may contribute to the initiation or relapse of chronic inflammation.

An intestinal obstructive loop model was used to induce bacterial overgrowth, accompanied by mucosal penetration and extraintestinal translocation. At early time points (6 hours) after ligation, MLCK-dependent TW MLC phosphorylation and BB fanning were associated with increased bacterial endocytosis. The possibility of paracellular or basolateral entry for microbes was ruled out because the TJ structures remained intact. Although bacterial sampling by M cells or dendritic cells may also contribute to microbial translocation,[35,36] intracellular microbes were observed mainly in epithelial cells in our study.

We found that IFN-γ–induced TW contraction and arc formation preceded caveolin-mediated bacterial endocytosis through cholesterol-rich lipid rafts. Previous reports documented IFN-γ overproduction by intraepithelial lymphocytes or lamina propria Th1 cells in association with the pathogenesis and disease severity of Crohn disease and celiac disease.[3,4] Other than the proinflammatory role, IFN-γ was linked with increased paracellular permeability by causing MLCK-dependent perijunctional actinomyosin contraction and ROCK-dependent junctional protein endocytosis.[18,37] The data from our group and others[8] further emphasize a critical role of low-dose IFN-γ in triggering transcellular bacterial passage before TJ damage, which may be responsible for relapse of chronic inflammation.

Whether the internalized microbial strains simply reflect their dominance in the gut lumen as bystanders trapped by microvilli or are associated with unknown virulent invasive factors remains elusive. Previous reports documented high prevalence of adhesive and invasive *E. coli* in patients with Crohn disease, patients with irritable bowel syndrome, and those undergoing colectomy.[38–40] These bacterial isolates are known to penetrate and survive intracellularly better than other nonpathogenic commensals when co-cultured with intestinal epithelial cells.[40] Further experiments on characterizing the virulent factors of endocytosed bacteria are currently under way and will provide information on host-microbial interaction.

The nonmuscle long MLCK (210 kDa) is the predominant isoform expressed in enterocytes with splice variants 1 and 2, which differed by the absence of a 69–amino acid region in the latter.[19] We found that knockdown of long MLCK leads to ablation of bacterial endocytosis in epithelial cells. The long MLCK-1 is involved in perijunctional actinomyosin contraction,[19] whereas the function of long MLCK-2 in enterocytes is currently unknown. Further research to verify specific roles of long MLCK-1 and -2 variants in response to IFN-γ activation is needed.

Conclusion

Our study reveals that apical bacterial internalization is regulated by IFN-γ–induced MLCK-dependent BB fanning. The understanding of intermicrovillous penetration and transcytotic pathways of commensal microbes may shed light on the development of therapeutic intervention to prevent relapse of chronic intestinal inflammation.

Acknowledgments

We thank the staff of the imaging facility at the First Core Lab and the AM2 of Disease Animal Research Center for their technical assistance.

Study concept and design: L.C.Y.; data acquisition: L.L.W., W.H.P., W.T.K., C.Y.H.; data analysis/interpretation: L.L.W., Y.H.N., K.S.L.; statistical analysis: L.L.W.; material and technical support: Y.H.N., K.S.L., J.R.T.; obtained funding: L.C.Y.; manuscript drafting and editing, literature research, and manuscript final version approval: all authors.

Supplemental Data

Supplemental material for this article can be found at *http://dx.doi.org/10.1016/j.ajpath.2014.05.003*.

References

1. Swidsinski A, Ladhoff A, Pernthaler A, Swidsinski S, Loening-Baucke V, Ortner M, Weber J, Hoffmann U, Schreiber S, Dietel M, Lochs H: Mucosal flora in inflammatory bowel disease. Gastroenterology 2002, 122:44–54
2. Kleessen B, Kroesen AJ, Buhr HJ, Blaut M: Mucosal and invading bacteria in patients with inflammatory bowel disease compared with controls. Scand J Gastroenterol 2002, 37:10034–10041
3. Forsberg G, Fahlgren A, Hörstedt P, Hammarström S, Hernell O, Hammarström ML: Presence of bacteria and innate immunity of intestinal epithelium in childhood celiac disease. Am J Gastroenterol 2004, 99:894–904
4. Sjöberg V, Sandström O, Hedberg M, Hammarström S, Hernell O, Hammarström ML: Intestinal T-cell responses in celiac disease - impact of celiac disease associated bacteria. PLoS One 2013, 8: e53414
5. Gareau MG, Jury J, MacQueen G, Sherman PM, Perdue MH: Probiotic treatment of rat pups normalises corticosterone release and ameliorates colonic dysfunction induced by maternal separation. Gut 2007, 56: 1522–1528
6. Engel DR, Koscielny A, Wehner S, Maurer J, Schiwon M, Franken L, Schumak B, Limmer A, Sparwasser T, Hirner A, Knolle PA, Kalff JC, Kurts C: T helper type 1 memory cells disseminate postoperative ileus over the entire intestinal tract. Nat Med 2010, 16:1407–1413
7. Samel S, Keese M, Kleczka M, Lanig S, Gretz N, Hafner M, Sturm J, Post S: Microscopy of bacterial translocation during small bowel obstruction and ischemia in vivo - a new animal model. BMC Surg 2002, 2:6
8. Clark E, Hoare C, Tanianis-Hughes J, Carlson GL, Warhurst G: Interferon gamma induces translocation of commensal Escherichia coli across gut epithelial cells via a lipid raft-mediated process. Gastroenterology 2005, 128:1258–1267
9. Smyth D, McKay CM, Gulbransen BD, Phan VC, Wang A, McKay DM: Interferon-gamma signals via an ERK1/2-ARF6 pathway to promote bacterial internalization by gut epithelia. Cell Microbiol 2012, 14:1257–1270
10. Wells CL, VandeWesterlo EM, Jechorek RP, Erlandsen SL: Effect of hypoxia on enterocyte endocytosis of enteric bacteria. Crit Care Med 1996, 24:985–991
11. Lewis K, Lutgendorff F, Phan V, Söderholm JD, Sherman PM, McKay DM: Enhanced translocation of bacteria across metabolically stressed epithelia is reduced by butyrate. Inflamm Bowel Dis 2010, 16: 1138–1148
12. Shifrin D, McConnell R, Nambiar R, Higginbotham J, Coffey R, Tyska M: Enterocyte microvillus-derived vesicles detoxify bacterial products and regulate epithelial-microbial interactions. Curr Biol 2012, 22:627–631
13. Danielsen EM, Hansen GH: Lipid rafts in epithelial brush borders: atypical membrane microdomains with specialized functions. Biochim Biophys Acta 2003, 1617:1–9
14. Kalischuk L, Inglis GD, Buret A: Campylobacter jejuni induces transcellular translocation of commensal bacteria via lipid rafts. Gut Pathog 2009, 1:2
15. Peterson MD, Mooseker MS: Characterization of the enterocyte-like brush border cytoskeleton of the C2BBe clones of the human intestinal cell line, Caco-2. J Cell Sci 1992, 102:581–600
16. Keller TC, Mooseker MS: Ca^{++}-calmodulin-dependent phosphorylation of myosin, and its role in brush border contraction in vitro. J Cell Biol 1982, 95:943–959
17. Keller TC, Conzelman KA, Chasan R, Mooseker MS: Role of myosin in terminal web contraction in isolated intestinal epithelial brush borders. J Cell Biol 1985, 100:1647–1655
18. Utech M, Ivanov AI, Samarin SN, Bruewer M, Turner JR, Mrsny RJ, Parkos CA, Nusrat A: Mechanism of IFN-γ-induced endocytosis of tight junction proteins: myosin II-dependent vacuolarization of the apical plasma membrane. Mol Biol Cell 2005, 16: 5040–5052
19. Clayburgh DR, Rosen S, Witkowski ED, Wang F, Blair S, Dudek S, Garcia JGN, Alverdy JC, Turner JR: A differentiation-dependent splice variant of myosin light chain kinase, MLCK1, regulates epithelial tight junction permeability. J Biol Chem 2004, 279:55506–55513
20. Wu CC, Lu YZ, Wu LL, Yu LC: Role of myosin light chain kinase in intestinal epithelial barrier defects in a rat model of bowel obstruction. BMC Gastroenterol 2010, 10:39
21. Wu LL, Chiu HD, Peng WH, Lin BR, Lu KS, Lu YZ, Yu LC: Epithelial inducible nitric oxide synthase causes bacterial translocation by impairment of enterocytic tight junctions via intracellular signals of Rho-associated kinase and protein kinase C zeta. Crit Care Med 2011, 39:2087–2098
22. Clayburgh DR, Barrett TA, Tang Y, Meddings JB, Van Eldik LJ, Watterson DM, Clarke LL, Mrsny RJ, Turner JR: Epithelial myosin light chain kinase–dependent barrier dysfunction mediates T cell activation–induced diarrhea in vivo. J Clin Invest 2005, 115: 2702–2715
23. Barakat FM, McDonald V, Santo JPD, Korbel DS: Roles for NK cells and an NK cell-independent source of intestinal gamma interferon for innate immunity to cryptosporidium parvum infection. Infect Immun 2009, 77:5044–5049
24. Hsiao J, Huang C, Lu Y, Yang C, Yu L: Magnetic resonance imaging detects intestinal barrier dysfunction in a rat model of acute mesenteric ischemia/reperfusion injury. Invest Radiol 2009, 44: 329–335
25. Chen TL, Chen S, Wu HW, Lee TC, Lu YZ, Wu LL, Ni YH, Sun CH, Yu WH, Buret A, Yu LC: Persistent gut barrier damage and commensal bacterial influx following eradication of Giardia infection in mice. Gut Pathog 2013, 5:26
26. Grossmann J, Walther K, Artinger M, Kiessling S, Steinkamp M, Schmautz WK, Stadler F, Bataille F, Schultz M, Schölmerich J, Rogler G: Progress on isolation and short-term ex-vivo culture of highly purified non-apoptotic human intestinal epithelial cells (IEC). Eur J Cell Biol 2003, 82:262–270
27. Muyzer G, de waal EC, Uitterlinden AG: Profiling of complex microbial populations by denaturing gradient gel electrophoresis analysis of polymerase chain reaction-amplified genes coding for 16S rRNA. Appl Environ Microbiol 1993, 59:695–700
28. Wang Q, Garrity GM, Tiedje JM, Cole JR: Naïve bayesian classifier for rapid assignment of rRNA sequences into the new bacterial taxonomy. Appl Environ Microbiol 2007, 73:5261–5267
29. Banerjee A, Yasseri M, Munson M: A method for the detection and quantification of bacteria in human carious dentine using fluorescent in situ hybridisation. J Dent 2002, 30:359–363
30. Tyska MJ, Mackey AT, Huang JD, Copeland NG, Jenkins NA, Mooseker MS: Myosin-1a is critical for normal brush border structure and composition. Mol Biol Cell 2005, 16:2443–2457
31. Lu YZ, Wu CC, Huang YC, Huang CY, Yang CY, Lee TC, Chen CF, Yu LC: Neutrophil priming by hypoxic preconditioning protects against epithelial barrier damage and enteric bacterial translocation in intestinal ischemia/reperfusion. Lab Invest 2012, 92: 783–796
32. Huang CY, Kuo WT, Huang YC, Lee TC, Yu LC: Resistance to hypoxia-induced necroptosis is conferred by glycolytic pyruvate scavenging of mitochondrial superoxide in colorectal cancer cells. Cell Death Dis 2013, 2:e622
33. Yu LC, Flynn AN, Turner JR, Buret AG: SGLT-1-mediated glucose uptake protects intestinal epithelial cells against LPS-induced apoptosis

and barrier defects: a novel cellular rescue mechanism? FASEB J 2005, 19:1822–1835
34. Al-Sadi R, Ye D, Dokladny K, Ma TY: Mechanism of IL-1β-induced increase in intestinal epithelial tight junction permeability. J Immunol 2008, 180:5653–5661
35. Swiatczak B, Rescigno M: How the interplay between antigen presenting cells and microbiota tunes host immune responses in the gut. Semin Immunol 2012, 24:43–49
36. Salim SY, Silva MA, Keita AV, Larsson M, Andersson P, Magnusson KE, Perdue MH, Söderholm JD: CD83+CCR7- dendritic cells accumulate in the subepithelial dome and internalize translocated Escherichia coli HB101 in the peyer's patches of ileal Crohn's disease. Am J Pathol 2009, 174:82–90
37. Bruewer M, Utech M, Ivanov AI, Hopkins AM, Parkos CA, Nusrat A: Interferon-gamma induces internalization of epithelial tight junction proteins via a macropinocytosis-like process. FASEB J 2005, 19:923–933
38. Sobieszczańska BM, Osek J, Waśko-Czopnik D, Dworniczek E, Jermakow K: Association of enteroaggregative Escherichia coli with irritable bowel syndrome. Clin Microbiol Infect 2007, 13:404–407
39. Reddy BS, MacFie J, Gatt M, Macfarlane-Smith L, Bitzopoulou K, Snelling AM: Commensal bacteria do translocate across the intestinal barrier in surgical patients. Clin Nutr 2007, 26:208–215
40. Martinez-Medina M, Aldeguer X, Lopez-Siles M, González-Huix F, López-Oliu C, Dahbi G, Blanco JE, Blanco J, Garcia-Gil JL, Darfeuille-Michaud A: Molecular diversity of Escherichia coli in the human gut: new ecological evidence supporting the role of adherent-nonvasive E. coli (AIEC) in Crohn's disease. Inflamm Bowel Dis 2009, 15:872–882

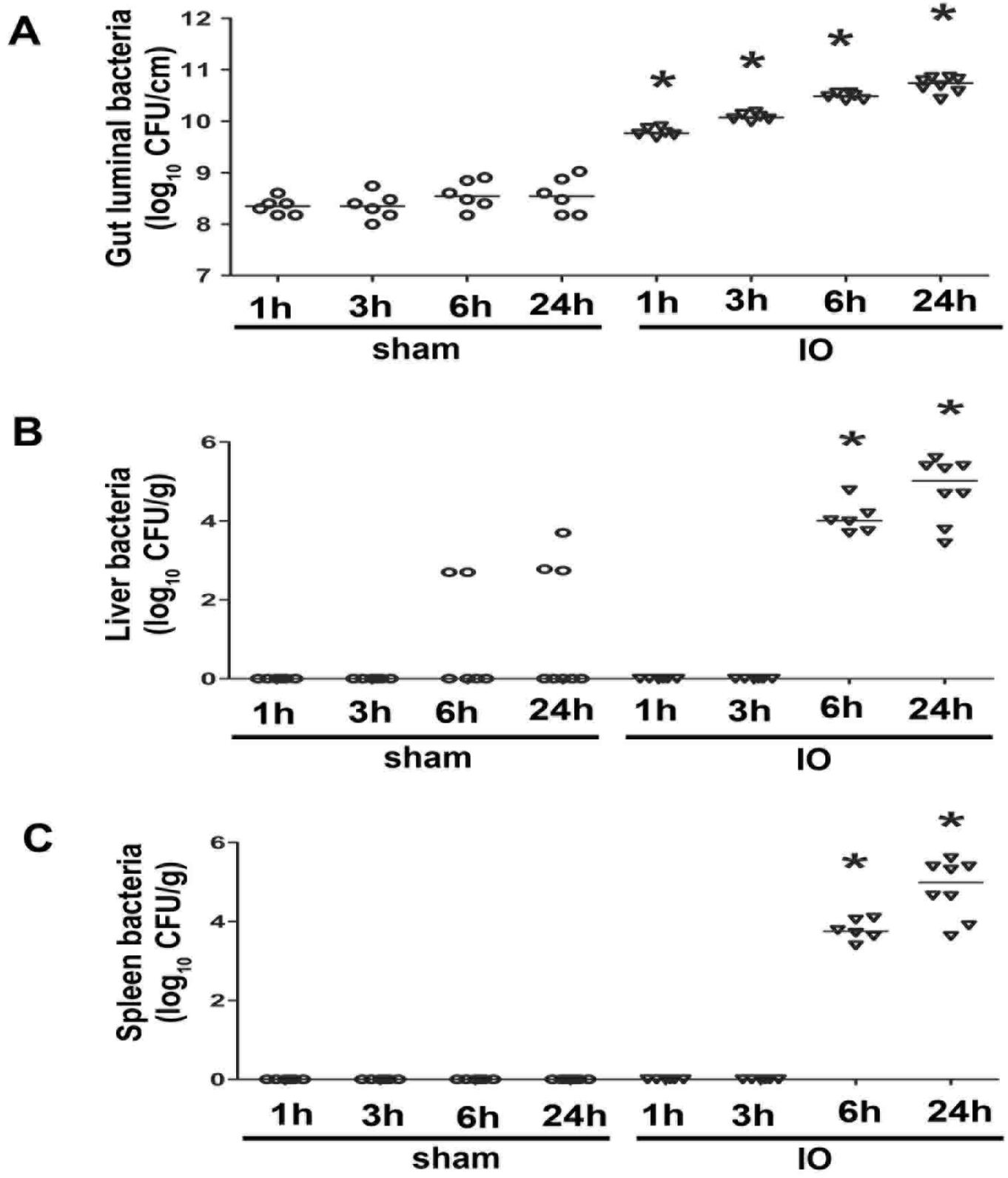
A
Gut luminal bacteria
(log10 CFU/cm)
12
11
10
9
8
7
1h
3h
6h
24h
1h
3h
6h
24h
sham
IO
B
Liver bacteria
(log10 CFU/g)
6
4
2
0
1h
3h
6h
24h
1h
3h
6h
24h
sham
IO
C
Spleen bacteria
(log10 CFU/g)
6
4
2
0
1h
3h
6h
24h
1h
3h
6h
24h
sham
IO

Figure S1

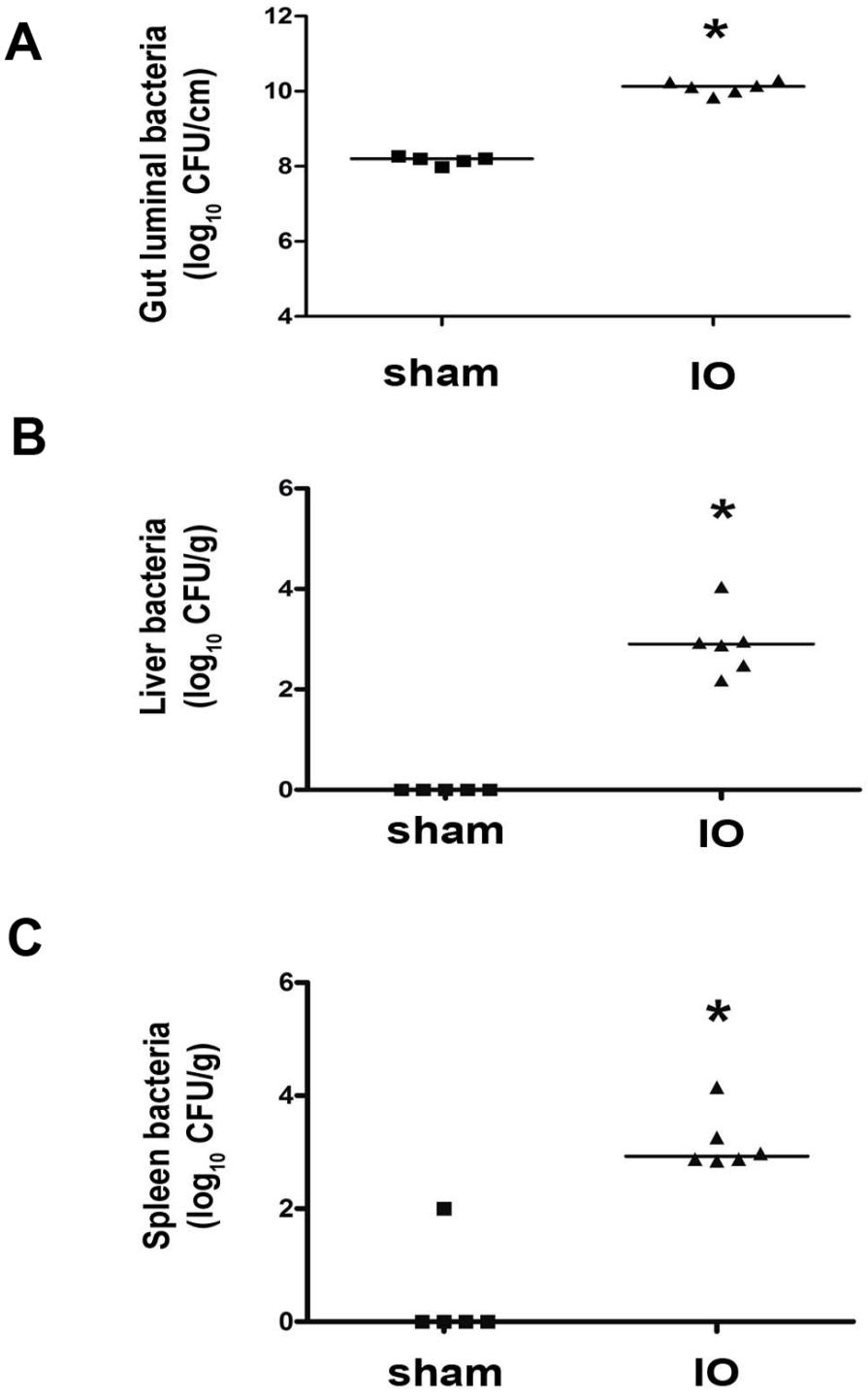
A
Gut luminal bacteria
(log10 CFU/cm)
12
10
8
6
4
*
sham
IO
B
Liver bacteria
(log10 CFU/g)
6
4
2
0
*
sham
IO
C
Spleen bacteria
(log10 CFU/g)
6
4
2
0
*
sham
IO

Figure S2

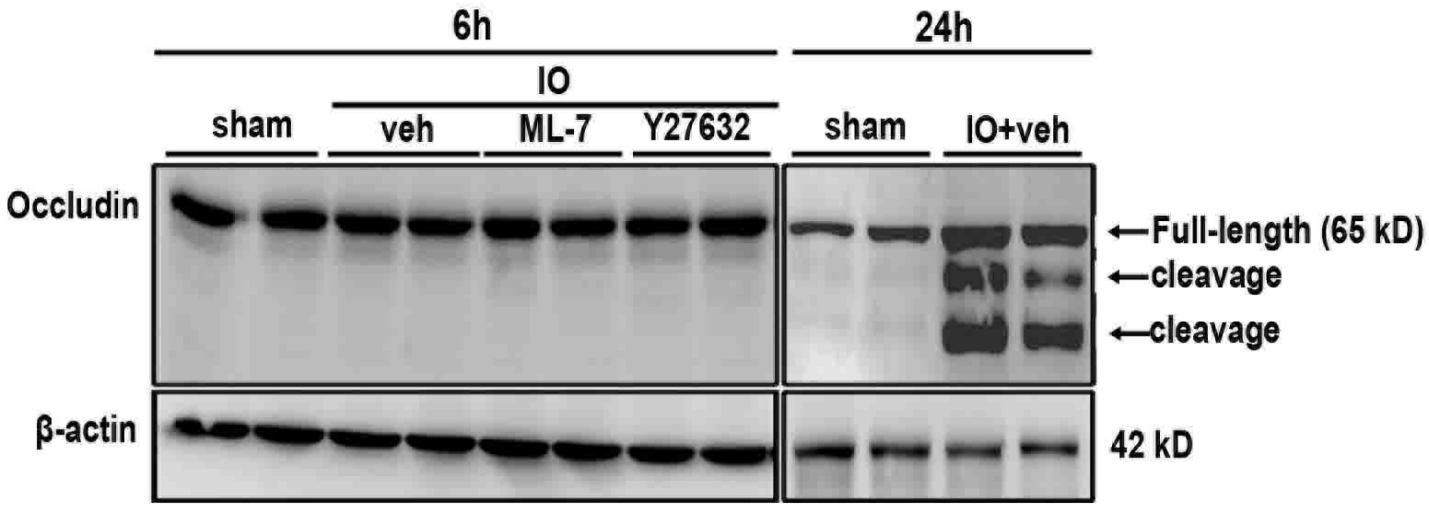
6h
24h
IO
sham
veh
ML-7
Y27632
sham
IO+veh
Occludin
β-actin
←Full-length (65 kD)
←cleavage
←cleavage
42 kD

Figure S3

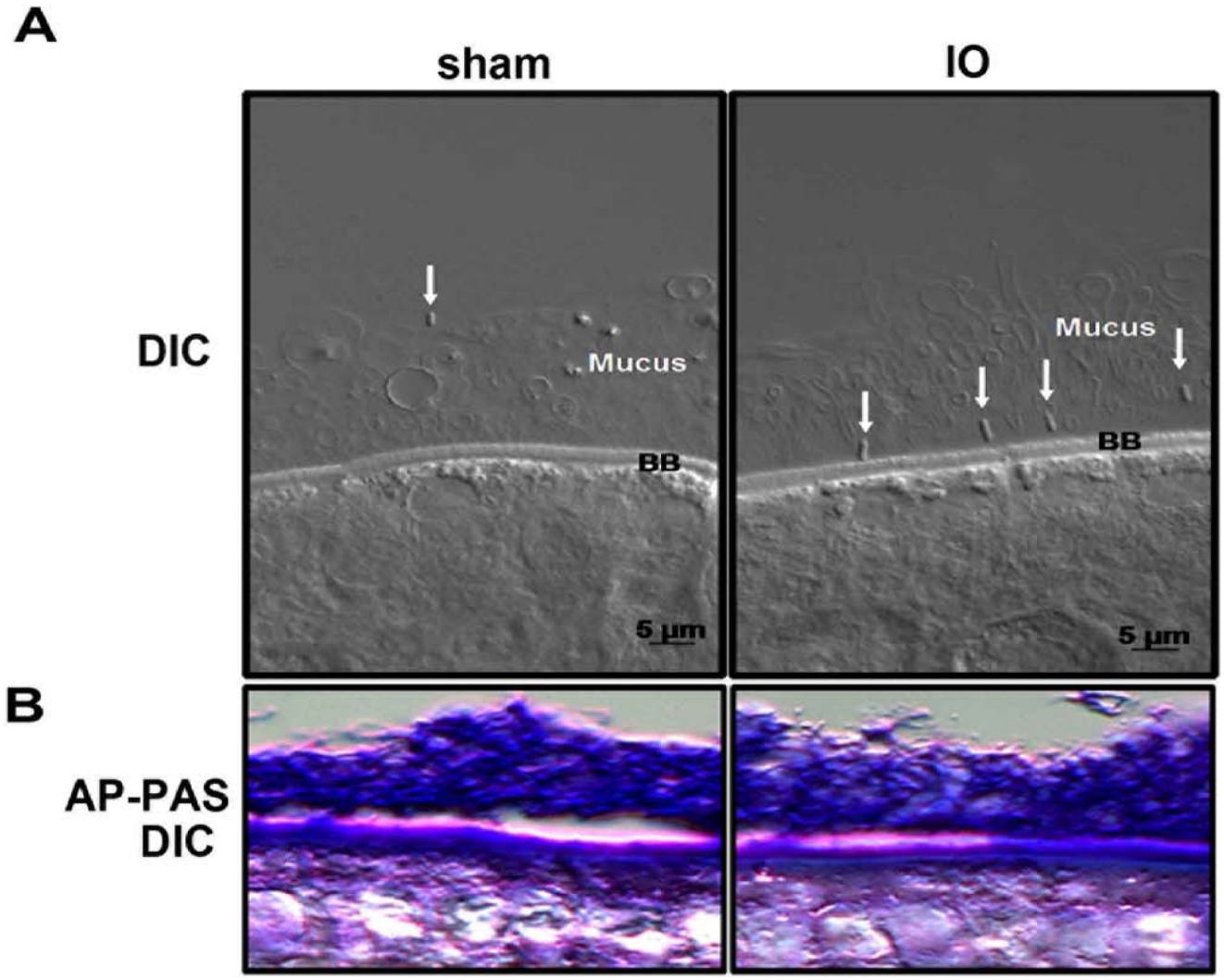

Figure S4

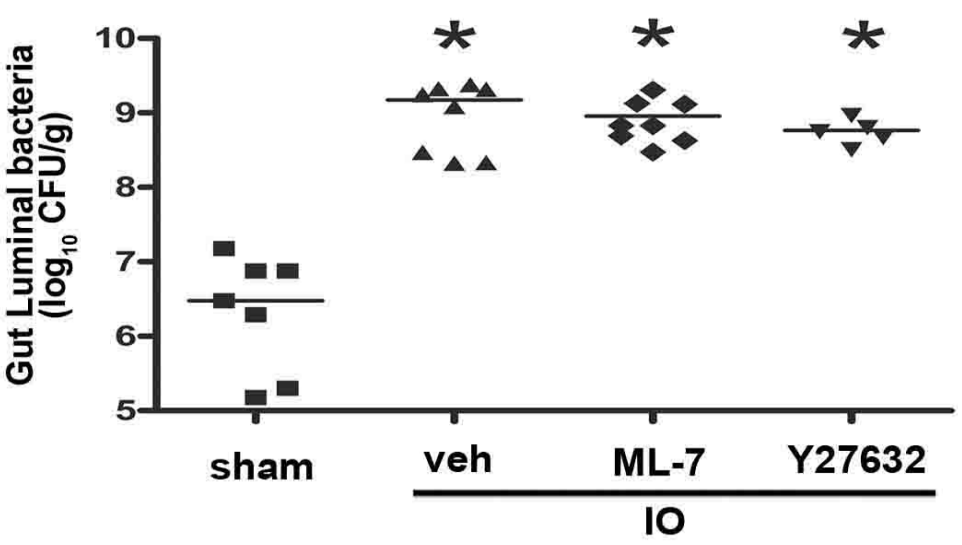
Gut Luminal bacteria
(log10 CFU/g)
10
9
8
7
6
5
*
*
*
sham
veh
ML-7
Y27632
IO

B

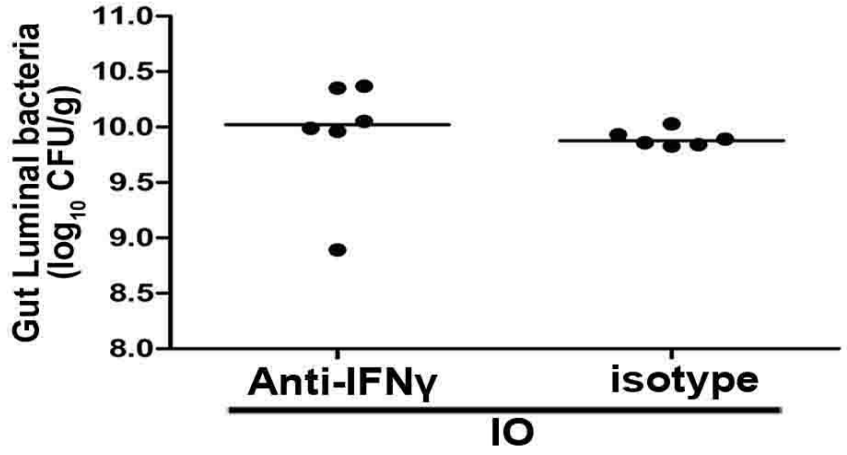
Gut Luminal bacteria
(log10 CFU/g)
11.0
10.5
10.0
9.5
9.0
8.5
8.0
Anti-IFNγ
isotype
IO

C

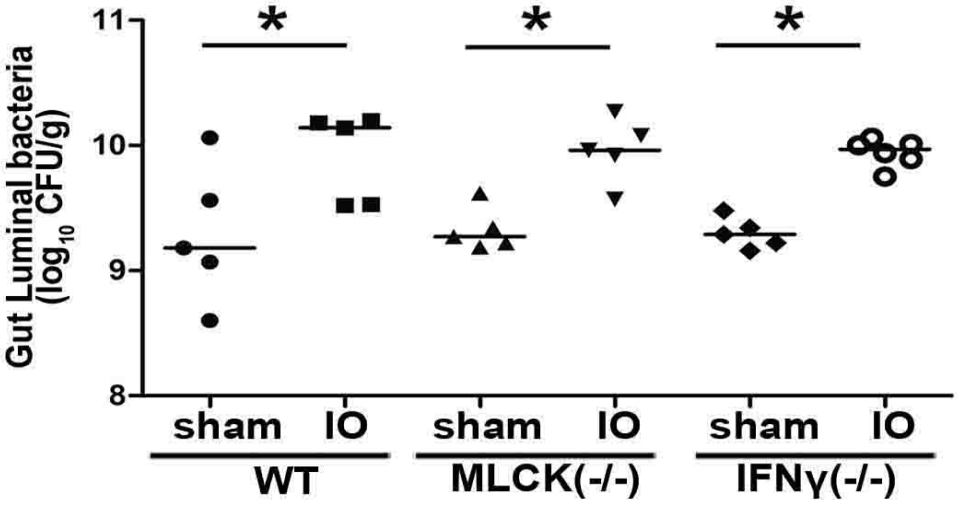
Gut Luminal bacteria
(log10 CFU/g)
11
10
9
8
*
*
*
sham
IO
sham
IO
sham
IO
WT
MLCK(-/-)
IFNγ(-/-)

Figure S5

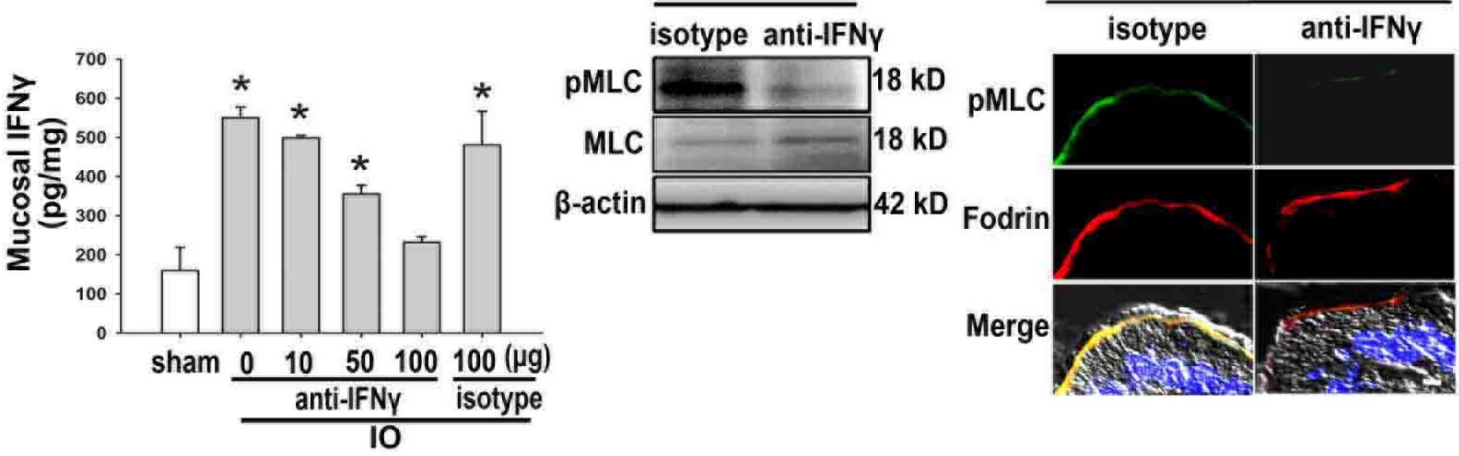
Mucosal IFNγ (pg/mg)
700
600
500
400
300
200
100
0
sham
0
10
50
100
100 (μg)
anti-IFNγ
isotype
IO
isotype
anti-IFNγ
pMLC
MLC
β-actin
18 kD
18 kD
42 kD
isotype
anti-IFNγ
pMLC
Fodrin
Merge

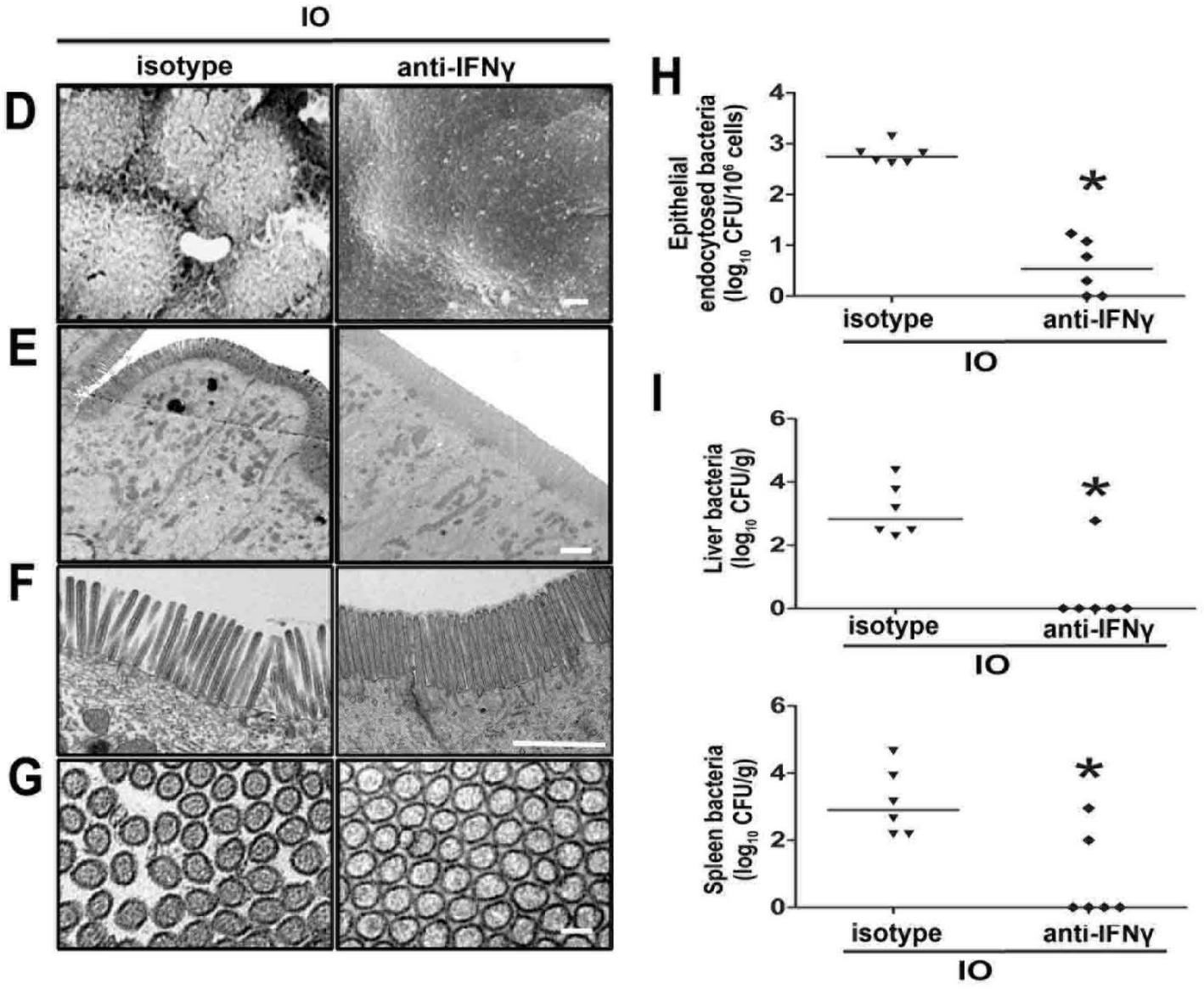
IO
isotype
anti-IFNγ
D
E
F
G
H
Epithelial endocytosed bacteria (log_{10} CFU/10^6 cells)
4
3
2
1
0
isotype
anti-IFNγ
IO
I
Liver bacteria (log_{10} CFU/g)
6
4
2
0
isotype
anti-IFNγ
IO
Spleen bacteria (log_{10} CFU/g)
6
4
2
0
isotype
anti-IFNγ
IO

Figure S6

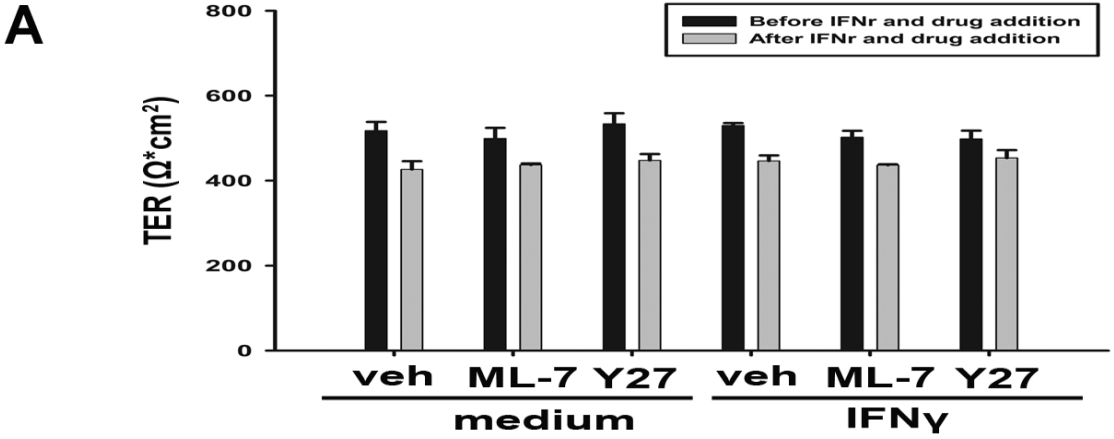
A
Before IFNr and drug addition
After IFNr and drug addition
TER (Ω*cm²)
800
600
400
200
0
veh
ML-7
Y27
veh
ML-7
Y27
medium
IFNγ

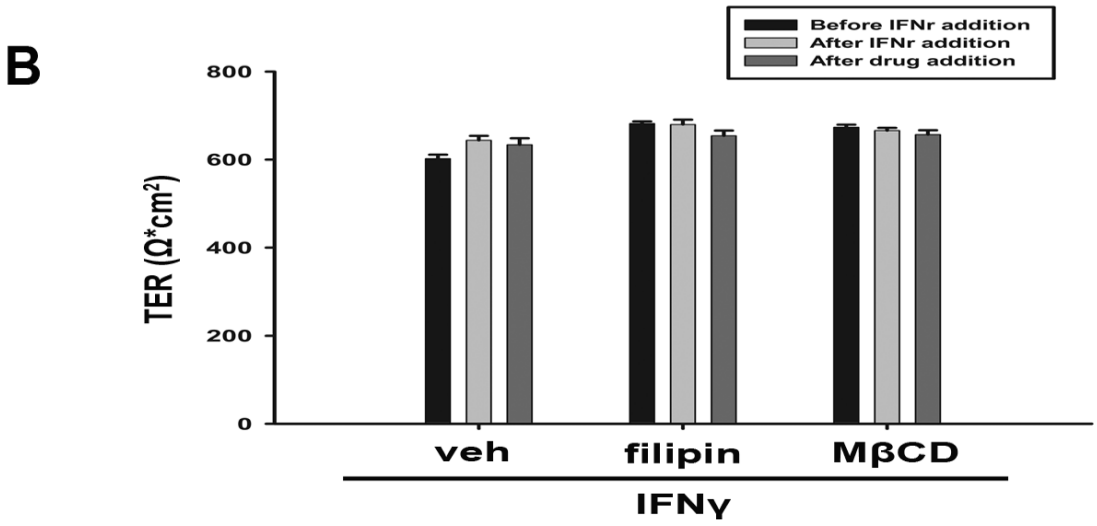
B
Before IFNr addition
After IFNr addition
After drug addition
TER (Ω*cm²)
800
600
400
200
0
veh
filipin
MβCD
IFNγ

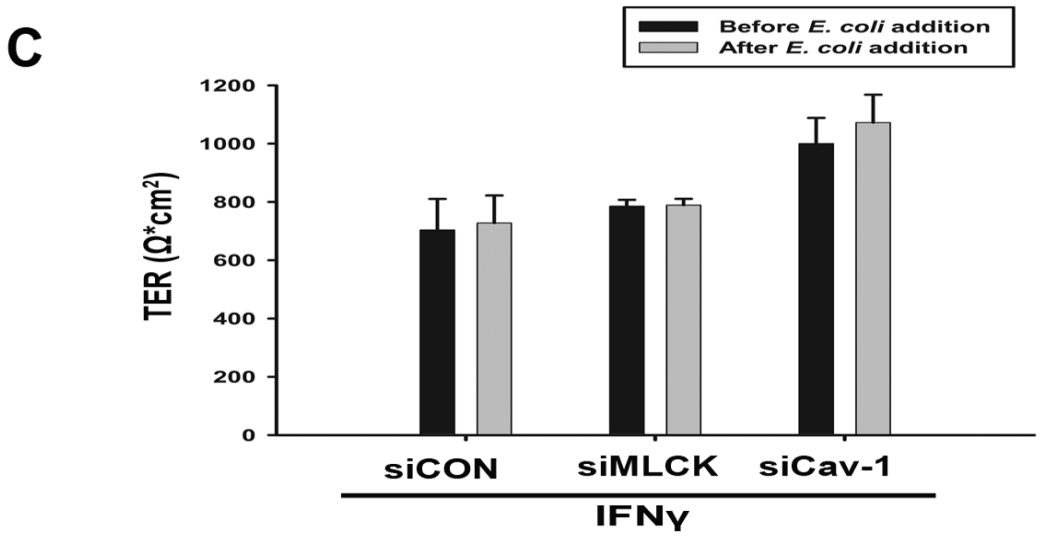
C
Before E. coli addition
After E. coli addition
TER (Ω*cm²)
1200
1000
800
600
400
200
0
siCON
siMLCK
siCav-1
IFNγ

Figure S7